MITLibraries
Document Services

Room 14-0551
77 Massachusetts Avenue
Cambridge, MA 02139
Ph: 617.253.5668 Fax: 617.253.1690
Email: docs@mit.edu
http://libraries.mit.edu/docs

DISCLAIMER OF QUALITY

Due to the condition of the original material, there are unavoidable flaws in this reproduction. We have made every effort possible to provide you with the best copy available. If you are dissatisfied with this product and find it unusable, please contact Document Services as soon as possible.

Thank you.

Some pages in the original document contain pictures, graphics, or text that is illegible.

ELECTROSTATIC DEFLECTION OF FREE-STANDING TUNGSTEN MICROBRIDGES AS A NOVEL MEANS FOR CHARACTERIZATION OF THIN FILM MECHANICAL PROPERTIES

by

S. Carolene Huguenin

Submitted to the Department of Materials Science and Engineering

in partial fulfillment of the requirements for the degree of

Master of Science

at the

Massachusetts Institute of Technology

May 6, 1994

© S. Carolene Huguenin 1994. All rights reserved.

The author hereby grants to MIT permission to reproduce and to

distribute copies of this thesis document in whole or in part.

Signature of Author ______________________________
Department of Materials Science and Engineering
May 6, 1994

Certified by ______________________________
Professor C. V. Thompson II
Professor of Electronic Materials
Thesis Supervisor

Accepted by ______________________________
Professor C. V. Thompson II
Professor of Electronic Materials
Chair, Department Committee on Graduate Students

Science

MASSACHUSETTS INSTITUTE OF TECHNOLOGY

AUG 18 1994

LIBRARIES

ELECTROSTATIC DEFLECTION OF FREE-STANDING TUNGSTEN MICROBRIDGES AS A NOVEL MEANS FOR CHARACTERIZATION OF THIN FILM MECHANICAL PROPERTIES

by

S. Carolene Huguenin

Submitted to the Department of Materials Science and Engineering

Massachusetts Institute of Technology

May 6, 1994

Abstract

Within the past decade, characterization of thin film mechanical properties has been a topic of particular interest to the device industries that require reliable magnetic, electronic, and optical thin films. The problem of mechanical characterization on the size scales used in contemporary microdevices, however, has only recently been addressed. Surface micromachining techniques, which arose from the process technologies of the microelectronics community, provide the ability to fabricate micron-scale electromechanical devices for measurement of film properties. This project involved the development of a fabrication process to produce free-standing tungsten microbridges for electrostatic deflection tests. Deflection structures, comprised of six hundred (1μm x 1μm x 1mm) CVD tungsten beams suspended 0.5 microns above a continuous electrode film of 50/50 wt. % titanium-tungsten, were utilized for C-V deflection measurements and destructive pull-in voltage determination. Design, processing, and electrical analysis of the test structures, as well as the theoretical basis for interpretation of electrostatic beam bending data, are described. Low yield of intact structures resulted from insufficient design tolerances, processing error, and the mechanical brutality of the liquid phase etch of the sacrificial dielectric. Recommendations for future efforts are suggested. Despite processing difficulties, a purely electromechanical technique for elastic modulus measurement is demonstrated.

Thesis Supervisor: Carl V. Thompson, II
Title: Professor of Electronic Materials,
Department of Materials Science and Engineering

Company Supervisor: Michael E. Thomas
Title: Senior Member of Research Staff, National Semiconductor Corporation

Table of Contents

Abstract 2

Acknowledgments 5

I. Introduction 6

II. Design of Test Structure 11

III. Fabrication 15

A. General Process Flow 15

B. Process Development 19

1. The PSG Etch Process 20

2. Integrity of the TiW Adhesion Layer 25

3. Sample Preparation Prior to PSG Etch 27

IV. Electrical Test and Measurement 28

A. C-V Deflection Measurements 28

B. Determination of the Pull-in Voltage 30

V. Results and Discussion 36

A. Process Results 36

1. Over-etch of the TiW Film 36

2. Photoresist Residue 37

3. PSG Step Coverage 39

4. Etch of Sacrificial PSG Film 41

5. The Tungsten Film 43

6. Appearance of Titanium-Tungsten Film 47

B. Electrostatic Deflection Results 47

1. Voltage-Capacitance Curves 48

2. The Pull-in Voltage 51

VI. Conclusions and Future Work 55

Appendix A: Video Tape: Voltage Index 57

References 58

Table of Figures

Figure 1. The Electrostatic Deflection Test Structure Geometry 12
Figure 2. The General Process Flow 16
Figure 3. Etch Nonuniformity of the HF Vapor Phase Process 21
Figure 4. Crystalline P Residue from HF Vapor Phase Process 22
Figure 5. Attack of TiW Via Foundation Film 25
Figure 6. Effective Spring Constant Model 31
Figure 7. Instability in the Capacitor/Spring Model 32
Figure 8. Beam Fixed at Two Ends 33
Figure 9. Pull-in Voltage Apparatus 35
Figure 10. Via Cross-Section Showing Etch of Silicon Nitride 37
Figure 11. Tungsten Beams with Photoresist Residue 38
Figure 12. Nodules on Tungsten Beams 39
Figure 13. Step Coverage Effects 40
Figure 14. Beam Shorted to Ground by Tungsten Cusp 41
Figure 15. Detached Via & Preferential Etch of PSG Around TiW 42
Figure 16. Attached Via & Preferential Etch of PSG Around TiW 43
Figure 17. Damage to TiW Film Following PSG Etch 44
Figure 18. Columnar Grain Structure 44
Figure 19. Capacitance vs. Applied Voltage, Tests 1-10 49
Figure 20. Capacitance vs. Applied Voltage, Tests 40-50 50
Figure 21. Elastic Modulus vs. Pull-in Voltage for s = 772.4 MPa 53
Figure 22. Plots of Equation 15 54

Acknowledgments

I would like to express my gratitude to Dr. Michael E. Thomas of National Semiconductor Corporation and Professor Carl V. Thompson of the Department of Materials Science and Engineering at M.I.T. for their guidance throughout this project. The majority of this work was conducted at National Semiconductor's Fairchild Research Center in Santa Clara, CA. Special thanks to Dr. Irfan Sadaat, Satoshi Sekigahama, Brian Daniels, and Dennis Rossman for their efforts, technical aid, and support during my internship in California. The efforts of Dr. Dah-Bin Kao and Dr. Gregory Scott in obtaining the electrical measurement equipment and transfer of data were also especially appreciated. On the other coast, Peter Osterberg and Raj Gupta of the Electrical Engineering and Computer Science Department at M.I.T. contributed greatly to my understanding of the pull-in voltage analysis through their time, patience and enthusiasm for this topic. Last, but certainly not least, I wish to thank my fiance, Claude Denton for his love and encouragement during the frustrating times.

I. Introduction

As processing technologies allow for smaller and more complex devices, understanding the mechanical properties of thin film components becomes an ever more critical reliability issue. Thin films often possess internal stress states, grain structures and preferential crystallographic orientations not found in bulk polycrystals. Mechanical properties are a manifestation of these microstructural issues, and therefore may be profoundly affected by the structural differences associated with reduced film dimensions, substrate interface effects, and varied deposition parameters. In order to optimize the reliability and durability of microdevice thin films, knowledge of the relationships between processing, microstructure, and the resulting mechanical properties is required.

Improvements in mechanical characterization techniques may lead to greater quantitative understanding of the correlations between microstructural qualities and mechanical behavior. The modulus of elasticity (E) and yield stress (σy) are materials constants of particular interest to thin film applications, since they describe the ability of the film to withstand mechanical stress. This thesis describes a system for measuring the mechanical properties of as-deposited thin films with particular emphasis on the determination of elastic modulus and the potential for measurement of yield stress.

The relationship between stress and reversible strain within a material is described by the elastic modulus. This mechanical characteristic is a macroscopic indication of interatomic bond forces. In general, the elastic modulus of thin films does not differ greatly from that of bulk material. However, preferential crystallographic orientation of grains, referred to as texture, may cause some variation in elastic moduli

for thin films composed of elastically anisotropic grains. [1] Several researchers have reported a thickness dependence for elastic moduli of films less than a few hundred nanometers in thickness. Claims have included an increased elastic modulus for gold films less than 4000 Å in thickness, [2] and a reduced modulus of elasticity for aluminum films of thicknesses less than 10 nm. [3] Also, investigation of the elastic modulus of nanocrystalline palladium has recently indicated an apparent decrease in the modulus with reduction in grain size. [4] Observations of these so-called elastic modulus effects are few and have received subdued reactions due to the large margins of error associated with the measurement techniques used in these studies. Improved mechanical characterization methods, such as the electrostatic deflection technique explored in this work, may allow for future confirmation or refutation of these results. Regardless of possible size dependent modulus effects, the ability to measure the elastic modulus of textured, elastically anisotropic thin film materials would provide a means for further investigation of the relationship between processing, microstructure, and resulting elastic properties of thin films.

The yield strength is the stress at which plastic deformation begins to occur within a material. Thin films exhibit enhanced strengths as a result of a variety of microstructural factors. Since dislocation motion is constrained by the surfaces and interfaces of the thin film, yielding within the polycrystalline film occurs through the motion of dislocation loops through grain lattices. The driving force for movement of these threading dislocations depends on the film thickness. [5] Grain boundaries act to hinder the motion of dislocations, although pile-up of dislocations at a grain boundary can cause the motion of imaging dislocations in neighboring grains. The Hall-Petch relation, which states that the strengthening of a polycrystal is proportional to the negative square root of the grain size, is derived from this physical situation. [6] Grain size strengthening, due to the fact that grain dimensions tend not to exceed the film

thickness, and strengthening due to the abundance of dislocations in thin films contribute to increased yield stress. [7] Treatment of the total yield stress as the sum of thickness and grain boundary dependent strengthening mechanisms provides results in excellent agreement with experimental data. [8, 9] In short, the yield strength of polycrystalline thin films has been well documented as a function of microstructural characteristics.

With the continuing reduction of feature sizes, the assumption that mechanical properties of device components can be approximated by those of larger samples has become increasingly inadequate. In response, the study of thin film mechanical properties has experienced a gradual evolution from classical macroscopic characterization methods. One of the most formidable problems facing investigators has been the challenge of testing a deposited film without also addressing the properties of the substrate material. The technique of bulge testing was developed as a means to apply classical mechanical test equipment to the problem of thin film properties. [10] Sample preparation involves the complete removal of the film from the substrate material, usually accomplished by either etch of the entire substrate, or deposition of the film over a sacrificial material that can be easily removed to free the film from the wafer surface. This technique requires delicate handling and large film areas to produce samples that can be mounted on O-rings and stressed with conventional bulk testing apparati. Although bulge testing has generated some insight into thin film mechanical behavior, plastic deformation of the film during substrate removal and other complicating factors of the sample preparation procedure have been significant sources of error.

Following in a similar evolution from traditional mechanical testing methods, microindentation techniques were developed. These approaches basically adopted the theoretical basis of the macroscopic Vicker (or Meyer) Hardness Tests, which involve

the indentation of a sample surface by a pyramidal (or semispherical) tip under an applied load and analysis of indent dimensions to render elastic and plastic flow properties. [6] Although similar to its macroscopic predecessors, microindentation reduced the indentor tip dimensions by three orders of magnitude, from millimeters to microns. Due to the indentation scale utilized in microindentation tests, individual constituents of multiphase alloys could be investigated, and the mechanical behavior of smooth film surfaces could be explored with considerably less sample preparation. Elastic relaxation and plastic characteristics of as-deposited films have been extensively studied through the use of microindentation over the past decade. [11] This technique requires significant film area (in order to indent using a matrix of many tips), knowledge of the effects of substrate properties on indentation results, and extremely smooth film surfaces. Although useful tools in the investigation of thin film mechanical properties, neither bulge testing nor microindentation has adequately addressed the problem of as-deposited film properties with exclusion of the substrate mechanical response.

The advent of micromachining processes presents a host of opportunities for new thin film geometries. Micromechanical device fabrication technologies arose from the maturation of standard microelectronics processing technologies. In the past few years, the ability to construct micron-scale, free-standing structures has been utilized to build micro-actuators, transducers, and switches for a wide variety of applications. Generally, these techniques center on the removal of sacrificial dielectric layers from below patterned metallic or semiconducting films in order to render free-standing products.

Recently, surface micromachining technologies have also been recognized as a vehicle for characterization of thin film mechanical properties. These techniques open

the possibility of testing of thin film microfeatures, as well as continuous thin films. Where continuous thin films are dimensionally constrained in one dimension, microfeatures such as high aspect ratio microbeams are constrained in two, film thickness and beam width. These reduced feature sizes may act to further lower the driving force for threading dislocation motion within the samples in a manner analogous to the dependence of yield stress on film thickness. In addition to dimensional differences, due to the free-standing nature of the structures, the built-in stresses of the initial film are relaxed transversely and longitudinally across the beam. [12] Thus, the stress state within a free-standing structure is unlike that of the continuous thin film from which it was fabricated. The ability to mechanically characterize patterned thin film features is a particularly important breakthrough since many device applications utilize micro-fabricated lines, cantilever arms, and diaphragms.

Again, progress has followed an evolutionary course. The mechanical deflection of thin film cantilever beams using microindentor tips was one of the first testing methods to address the problems posed by the presence of the substrate material and reduced sample feature sizes in the study of thin film mechanical properties. [13] Although revolutionary in its departure from classical materials testing apparati, the mechanical deflection technique remains limited to sample dimensions at least one order of magnitude greater than those used in contemporary microdevices, and is highly dependent on the ability of the indentor tip to apply force, measure deflection, and maintain a constant position on the cantilever surface. These limitations can be overcome through a purely electrical force/deflection measurement system. Techniques utilizing the application of electrostatic forces to micromechanical structures for the purposes of materials characterization have only recently been explored. [14] The application of electrostatic force to free-standing microbeams in order to obtain

materials properties through analysis of beam bending data is the subject of the following work.

II. Design of Test Structure

The test structure fabricated for the electrostatic deflection testing is depicted in Figure 1. The structure consisted of 600 identical, tungsten beams that spanned a 1 mm distance between two contact pads. The beams were 1μm in thickness, 1μm (or 1.5μm) in width, and 1mm in length, with an interbeam spacing of 2.0 μm. The zigzag shape along the ends of the beams was included in an effort to lessen stress concentrations at the beam/pad junctions. The beams were suspended 0.5 μm above a continuous, 900 Å thick film of titanium-tungsten which was electrically isolated from the tungsten beams and pads. The titanium-tungsten film served a second purpose in this design as the adhesion promoting layer beneath the tungsten contact pads, as illustrated in Figure 1(c). The various titanium-tungsten features were separated by a 1 μm space to assure electrical isolation of the beam structure and the underlying electrode. All dimensional specifications allowed for spatial lithography errors up to 0.25μm. There were effectively three contact pads within the structure. The long tungsten pads having dimensions of 1.8mm x 120μm were sufficiently large for contact with standard probe pins. While the two tungsten pads were a common circuit node, the third contact pad was a 120μm x 120μm extension of the titanium-tungsten electrode film that was electrically isolated from the tungsten structure.

Figure 1. The Electrostatic Deflection Test Structure Geometry

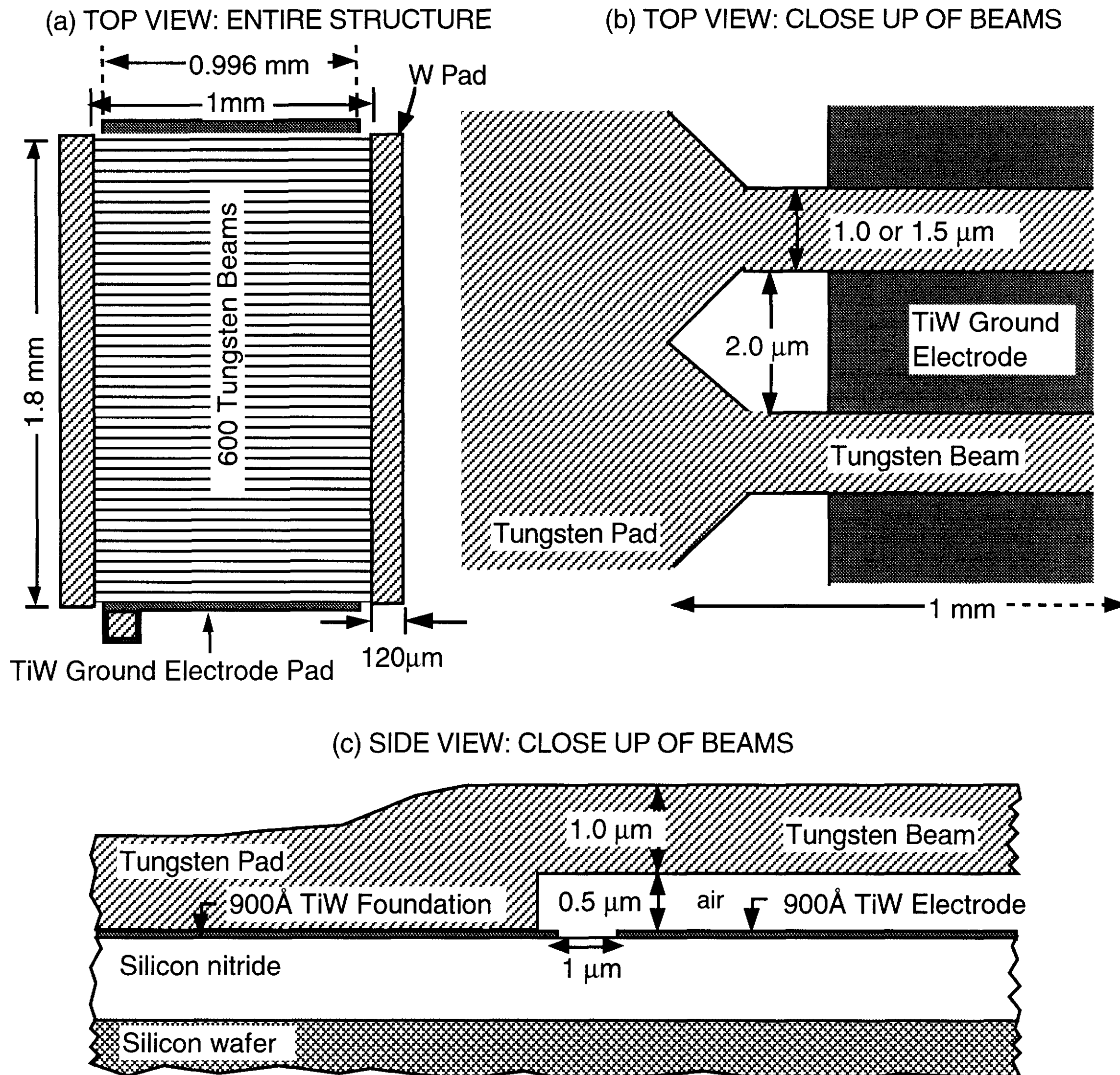

This test structure was designed to enable the application of electrostatic force to tungsten microbeams and permit measurement of induced beam deflections through changes in overall capacitance. Since capacitance varies in proportion to the areas of the electrodes and inversely with the distance between them, it was necessary to create a structure consisting of many microbridges suspended a small distance above the lower electrode to obtain measurable changes in capacitance. A 0.5 µm vertical gap was chosen based on process considerations, which involved the deposition of the sacrificial dielectric over the patterned titanium-tungsten film. Calculation of the capacitance of a

$1\mu m \times 1\mu m \times 1mm$ line in a parallel beam geometry was conducted utilizing the following idealized expression for an infinite parallel plate capacitor with air dielectric, in which ε_o is the permittivity of free space; A is the area of the beam parallel with the TiW film surface given by the product of the beam length and width; and d represents the vertical distance between the beams and the ground electrode surface:

$$C = \frac{\varepsilon_0 A}{d} \ . \qquad \text{(Eq.1)}$$

Letting d equal $0.5\mu m$, a value of 1.77×10^{-2} pF per line was computed. Since the parallel plate approximation ignores the contribution of the fringing electric fields at the beam edges, the calculation underestimates the capacitance of the structure. A structure with six hundred, $1\mu m$ wide lines was chosen to guarantee an initial capacitance of at least the 10pF required for measurement reliability.

The 600 beam structure was adopted for both the 1 μm and 1.5 μm wide beam structures, since the larger device would remain well above the minimum capacitance limitations of the measurement equipment and mask layout was facilitated by using a common geometry. The deflection structure with 1.5 μm beam widths was added to facilitate comparison of deflection results to data from other electromechanical devices that were not directly part of this project. Variation of the beam width was not anticipated to be an important factor in the utility of the test structure; the 1 μm structure was included in the mask to assess the impact on processing yield associated with the reduction in beam dimensions.

The design of the electrostatic deflection structure required three lithography steps, each utilizing a separate masking layer. The titanium-tungsten foundation and electrode regions were shaped by the first mask, which was a bright field mask. The second lithography step utilized a dark field mask to pattern holes in the sacrificial

dielectric for the anchored regions of the tungsten structure. Lastly, a second bright field mask defined the tungsten beams and pads.

In order to make realistic approximations for the initial capacitance of the beam structures, the effects of the fringing fields were taken into account. Using microstrip capacitance equations derived from the Schwarz-Christoffel transformation for an "almost parallel plate" capacitor, approximate capacitance values for the vertical deflection structures were calculated. [15] The geometry of the vertical deflection structures designed in this experiment had a w/d quotient of 2 and 3 for the 1μm and 1.5μm wide beams respectively. For situations where w/d>1, reference [15] gives the error of this numerical technique to be within 1 percent for a single line suspended over a ground plane. Capacitance values for individual beams were calculated from these equations and multiplied by the total number of beams to obtain approximate capacitance values for entire beam array; the implicit assumption of a linear relationship between single and multiple beams introduced additional error. The table below contains the data found through this approach as well as the capacitance values determined through the parallel plate approximation, which completely ignores fringing effects.

	Structure A 1.0μm beam width	Structure B 1.5μm beam width
Parallel Plate:	10.6 pF	15.9 pF
Stripline:	21.9 pF	29.9 pF

These capacitance values revealed that the contributions due to fringing of the electric fields surrounding the beams were significant. In fact, the estimated capacitance was essentially double the value determined by the infinite parallel plate simplification. Using a similar technique with the commercial two-dimensional finite element electric field simulator Electro™, an analysis was conducted to compare the capacitance of one, three and five electrically-connected 1.5 μm beams suspended 0.5 μm above a ground plane. A curve fit to the resulting data lead to a capacitance of 28.1pF when the number

of beams equaled 600. Since this estimated value is in keeping with that obtained from the stripline approximation, initial capacitances of approximately 20pF and 28pF were expected for the 1.0μm and 1.5μm structures respectively.

III. Fabrication

A. General Process Flow

The starting materials in the fabrication process for the electrostatic deflection test structures were six-inch silicon wafers upon which a 1.2μm silicon nitride film had been deposited and two alignment marks etched. The silicon nitride film was grown through a plasma enhanced chemical vapor deposition process. This nitride layer was included for purposes pertaining to structures included in the mask design that were not directly part of this project. The alignment marks were etched through the silicon nitride film; these deep trenches, which are comprised of sets of orthogonal hatch-marks, aid in photomask alignment for lithography. The entire fabrication process was conducted in a class 10 clean room, with the exception of the final step which involved the removal of the sacrificial glass film.

The first process in the fabrication sequence was the sputter deposition of a 900Å (± 90Å) thick film of 50/50 weight percent titanium-tungsten (TiW). Using a Varian 3290, the titanium-tungsten was sputtered after a brief rf etch employed to prepare the TiW target as well as the wafer surface. Figure 2 depicts the fabrication process for the electrostatic deflection structures beginning with the sputtering of the titanium-tungsten thin film. The titanium-tungsten layer was utilized in this process to promote adhesion of the tungsten to the nitride surface and to serve as the electrode surface below the suspended beams.

Figure 2. The General Process Flow

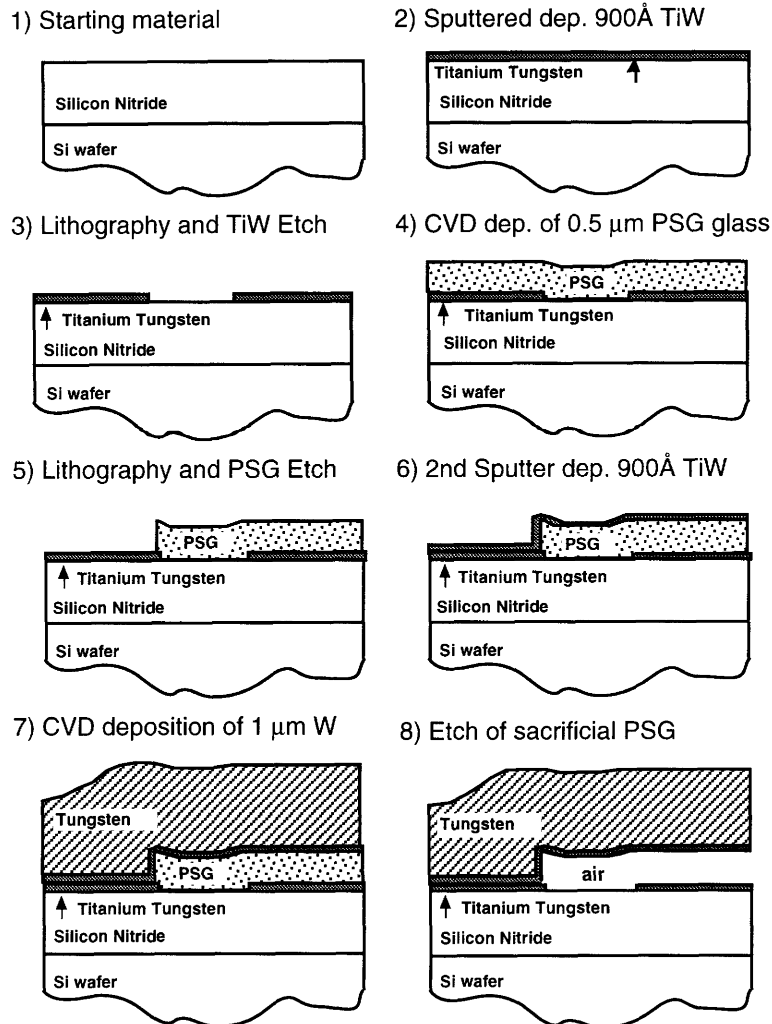

The titanium-tungsten film was then patterned using a bright-field photomask to produce the via foundation and bottom electrode geometries required in the layout. The lithography step utilized a 1.8μm spun-on film of positive photoresist. Following the developing and hard bake of the photoresist, the portions of the TiW film not covered by the protective polymer coating were removed using an Applied Materials Reactive Ion Etching System. A gas flow mixture containing CF_4 and a DC bias fueled and ignited the plasma for the etch process. Photoresist was removed through a succession of asher cleans, which essentially burned away the remaining photoresist, followed by a deionized

water rinse. Resist strippers containing sulfuric acid were purposefully avoided at this stage of the process due to titanium-tungsten's susceptibility to chemical attack by sulfuric acid.

A chemically vapor deposited film of phosphosilicate glass, 5000Å (± 200Å) in thickness, was grown over the wafer surface. This process was conducted within a Novellus Chemical Vapor Deposition Reactor maintained at a gas mixture of roughly 2% phosphine in nitrogen and flowing silane, at a temperature of 400°C. The phosphorus-doped glass was utilized as the sacrificial dielectric material due to earlier successes which had utilized a 3µm sacrificial film of PSG for a similar surface micromachining purpose. [16]

Due to the topography of the patterned TiW surface and the conformal nature of the chemically vapor deposited glass film, the shape of the tungsten beams was somewhat affected. The slight curvature of the tungsten beams over the TiW steps is represented in the diagrams of Figure 2. This downward deviation within the beam was not expected to be a problem since the thickness of the PSG layer deposited was over five times the step height. In addition, this aberration affected only the first and last micron of the 1mm long beam. Although the tungsten beams produced through this process appeared slightly warped, the beam-to-electrode distance remained constant along the entire beam length. One possible solution to the nonplanarity of the PSG glass would be to reflow the glass after the deposition. However, such a process would alter the overall thickness of the glass and therefore change the spacing of the tungsten beams from the titanium-tungsten electrode surface. Since the vertical distance must be known for analysis of beam deflection data, the PSG glass underwent no planarizing thermal treatments following deposition.

Having formed the PSG film, a second lithography step was required to define the geometry of the anchored areas of the test structures. A dark field mask was used to expose only those areas of the glass which were to be subjected to the etchant. Holes for the contact pads were cleared of phosphosilicate glass. This etch process was conducted in a LAM 4500 High Pressure Plasma Oxide Etcher that utilized a chemistry of Ar, CHF_3, and CF_4 to remove the 5000Å of PSG from the selected areas. The TiW adhesion layer provided an etch endpoint for this process. The photoresist was stripped using a series of asher cleans and an hour bath in an 80°C solvent solution composed of n-methyl pyrolidone in ethanol.

Again a 900Å titanium-tungsten adhesion layer was sputtered onto the wafer surface. The process described earlier, including the predeposition rf etch, was repeated. The vertical walls of the contact holes were not covered with as much TiW as the horizontal surfaces, due to the less conformal deposition process. A one micron thick film of CVD tungsten was then grown along the surface of the wafer and walls of the contact holes in an Applied Materials 5000, "warm-wall" reactor at 400°C. This CVD process was hydrogen rich and therefore the growth of the tungsten film was within the mass flow limited regime. A film with obvious surface roughness on the order of 0.25μm and a resistivity of 9.5μΩ/cm was produced. The properties of this film are considered further in the results section of this paper.

The last lithography step in the construction of the electrostatic deflection structures was patterning of the tungsten beams as called for in the mask design. Again, a surface layer of positive photoresist was exposed to a bright field mask in order to transfer the geometry of the tungsten features. Once the resist was developed and baked, the tungsten and titanium-tungsten films were removed by a second reactive ion etch process. An Applied Materials reactive ion etcher was again utilized. However, this

time a chlorine and sulfur hexafluoride mixture was employed to produce the proper plasma chemistry.

The tungsten/titanium-tungsten etch was the last fabrication process conducted in the clean room environment. Since failures of free-standing beams inadvertently produce small particulates (i.e. loose tungsten beams), all subsequent processing was conducted in the chase area of the fabrication facility.

The removal of the PSG glass from below the patterned tungsten film was the final process in the fabrication sequence. For lack of a more gentle etch technique, a liquid phase etch of 10:1 HF was employed to remove the glass from the wafer surface. The proper etch time in 10:1 HF for complete removal of the 0.5μm PSG film was approximately 1 minute and 15 seconds. Next, the wafer was placed in deionized water for 30 seconds and in isopropyl alcohol for an additional 30 seconds. Once removed from the alcohol, the samples were dried at approximately 70°C for 30 minutes. Following dehydration, the fabrication process for the electrostatic deflection structures was complete.

B. Process Development

Prior to this study, single tungsten bridges were fabricated as part of a separate series of experiments. The earlier structures consisted of individual bridges suspended 3μm above the wafer surface. With the exception of the deposition and etch of a thicker sacrificial glass film, these earlier structures utilized a similar fabrication sequence to that of the deflection structures of this project. Although many aspects of the earlier process were directly applicable to the requirements of the new design, alteration and improvement efforts were required. The etch of the sacrificial dielectric proved to be a

major challenge. Earlier work revealed extremely low yields from this processing step. The experiences and several unetched samples from the previous efforts were utilized in order to experiment with alternative etch techniques as well as further explore the variables of the older process. In addition, micrographs of the earlier structures indicated possible chemical attack of the TiW adhesion film during processing The removal of the sacrificial PSG layer and the durability of the TiW adhesion layer were explored at this time.

1. The PSG Etch Process:

The etch of the sacrificial PSG film is one of the most problematic components of the fabrication sequence. Several factors complicate the removal of the glass. First of all, free-standing beams are delicate structures that may not withstand the forces, viscous or otherwise, which are intrinsic to chemical processes. Also, etched and unetched sections along the length of the tungsten beams are often temporarily produced during the PSG removal process. Transient stress gradients caused by partial clearing of the glass film may arise within the tungsten geometries and induce structural failures. These problems are compounded by the fact that failures in one structure tend to physically harm neighboring devices. A single broken structure may scatter tungsten beams across the entire wafer surface causing short circuits in otherwise intact structures.

In previous work, a liquid phase etch of 10:1 HF was utilized. Observations of low yield due to structural damage incurred during the PSG removal suggested the need for a less violent etch process. Under this impetus, a gas phase etch process was investigated. A vendor company claiming to have such a process was contacted and supplied with partially processed wafers from the previous crosstalk measurement study. This HF vapor etch process involved a 49% HF solution heated to 35°C within a

reactor system designed for continuous recirculation of the vapor across the wafer surface. The seven wafers submitted to the vendor underwent varied etch times and were returned.

Figure 3. Etch Nonuniformity of the HF Vapor Phase Process

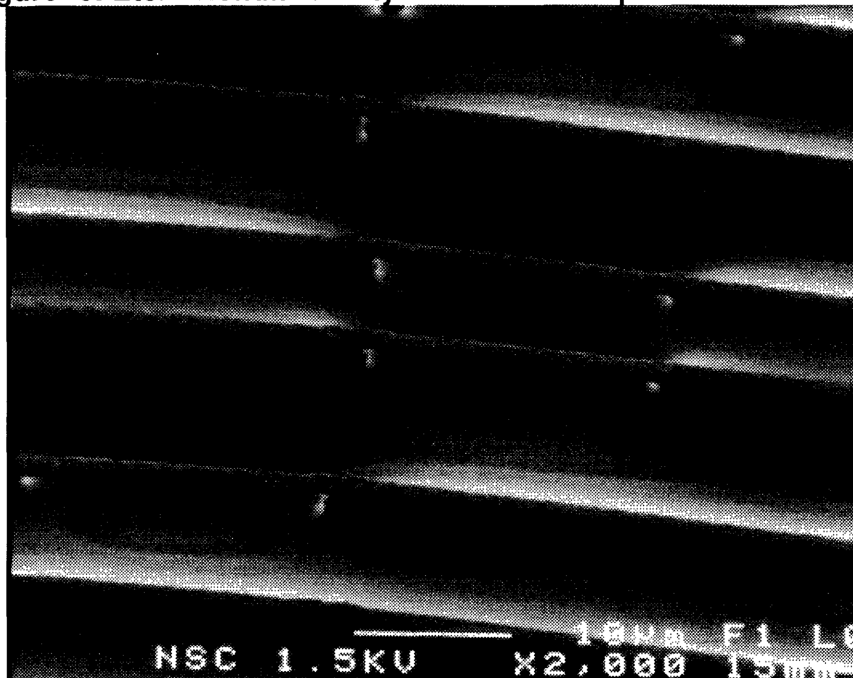

Inspection with a scanning electron microscope revealed poor uniformity in the etch process as well as a residue problem as depicted in Figure 3 and Figure 4. The canyon-like topography observed on several of the samples suggests that the etch process was not completely gas phase; condensation of the etchant on the wafer surface would explain these surface features. Regardless of the processing time, etch nonuniformity was evident on each sample. In some cases pitting into the underlying silicon nitride film was found immediately adjacent to areas covered by phosphosilicate glass. Several of the wafers exhibited further defects due to the presence of a residual material that had nucleated on the tungsten beams and even under the large tungsten pads. Using electron diffraction spectroscopy the dark crystalline residue was identified as phosphorous. The reason for the growth of the phosphorus crystals on some, but not all

of the wafers was not explored. Considering the poor results from each of the test samples, further attempts to utilize a gas phase etch process were abandoned.

Figure 4. Crystalline P Residue from HF Vapor Phase Process

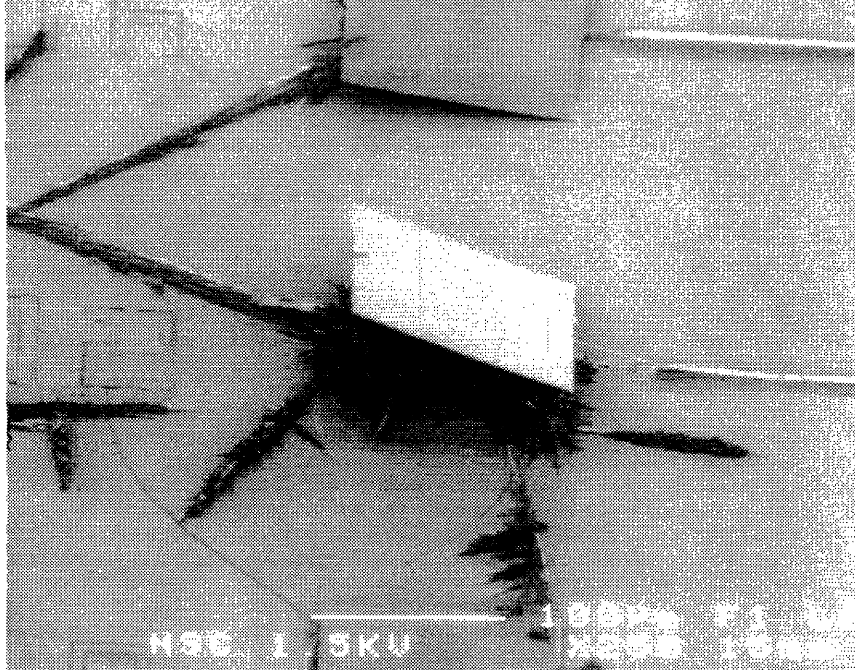

The return to a 10:1 HF liquid phase etch required consideration of the glass etch rate, since previous work had reported questionable results. The PSG timed etch experiments utilized during the fabrication of the earlier structures indicated a non-linear etch behavior in respect to time. Since the previous work had employed a thicker glass film and therefore longer etch time, a new series of etch rate tests was necessary to determine the etch time required for the removal of the half micron thick phosphosilicate glass. In order to conserve fabricated wafers, a six inch wafer with a 3 μm thick, blanket film of PSG above a 5,000Å film of silicon dioxide was subjected to a series of timed etches in 10:1 HF. The following table summarizes the calculated etch rates for the continuous glass film.

Etch Rate Data for the Blanket PSG Film

Sample Number	Etch Time (min:sec)	Av. Etch Rate (Å/min.)
1	1:00	3,966
2	1:30	5,295
3	2:00	5,765

The thickness of the PSG was determined through use of a Nanospec ellipsometer before and after each etch. For each sample five independent ellipsometry measurements were conducted at each phase of the experiment. In the table above, the column on the right represents the difference between the final and initial thicknesses divided by the total etch time. The apparent acceleration of the etch rate is a particularly interesting aspect of this data. In fact, the etch rate during the last minute of the two minute etch was 7,563 Å/min, almost twice the rate during the first minute. In addition to ellipsometry measurements, a Dektak Profilometer was used to obtain the step height of the etched glass by masking a small area prior to the etch. This measurement was conducted after two minutes in the etchant and suggested a higher overall etch rate of 7960 Å/min.

Taking into account the dubious information gained through the blanket PSG study, experimentation with cleaved sections of a processed wafer was then attempted. Unlike the previous samples, these wafer sections consisted of a 0.5µm thick, phosphosilicate glass film below a patterned, 1.0 µm thick tungsten film. A large range of etch times, between 25 seconds and 90 seconds, was examined in response to the 0.3 - 0.7 µm/min rates from the blanket PSG films.

Samples generated by the deflection structure fabrication process were gently placed in a 10:1 HF bath for the indicated time, deionized water for 30 seconds, a container of isopropyl alcohol for 30 seconds, and finally to an oven for 30 minutes at approximately 70°C to dry . The object of this approach was to minimize any

unnecessary forces such as extreme turbulence in the solutions or an N_2 blow dry. Etch rate data for the partially exposed PSG film revealed the following trend:

Etch Rate Data for the Below Patterned Metal Film

Sample Number	Etch Time (min:sec)	Av. Etch Rate (Å/min.)
1	0:25	2,484
2	0:30	2,154
3	0:35	2,310
4	0:45	1,650
5	0:45	1,445
6	1:00	1,292
7	1:15	956
8	1:30	833

As before, the etch rates in the right column were derived from ellipsometry performed before and after etching; special care was taken to perform measurements in the open PSG regions of the die to avoid optical effects caused by the tungsten film. As implied by the data, the etch rate for the phosphosilicate glass contained below the patterned tungsten is significantly slower than that of a surface PSG film. In fact, these results indicate that a one minute etch of a blanket film will have an etch rate three times faster than that of the sacrificial PSG layer of the deflection structures. Also, note the trend toward an etch rate deceleration over time; this is directly opposed to the enhanced etch rates observed with extended etches of the continuous PSG film.

In order to double check the accuracy of the ellipsometry technique, the samples were inspected using a scanning electron microscope. Visual inspection of the beams showed less than adequate PSG removal for all but the 1.25 minute and 1.5 minute tests. Etch nonuniformity across the wafer surface was again noted, although these variations were much more subtle than the islands and canyons left by the earlier gas phase process.

Physical evidence obtained through S.E.M. observation confirmed the inaccuracy of the ellipsometry measurements of these complex geometries. Since the 1.5 minute

etch appeared largely successful in clearing the PSG film from below the patterned tungsten film, the etch rate of 833Å/min reported above is obviously unrealistic; a more likely etch rate would be approximately 3,333Å/min. In considering that ellipsometry yielded reasonable etch rates for the blanket PSG film samples, the errors evident in the later experiments were most likely the effect of reflections from nearby patterned tungsten features.

Figure 5. Attack of TiW Via Foundation Film

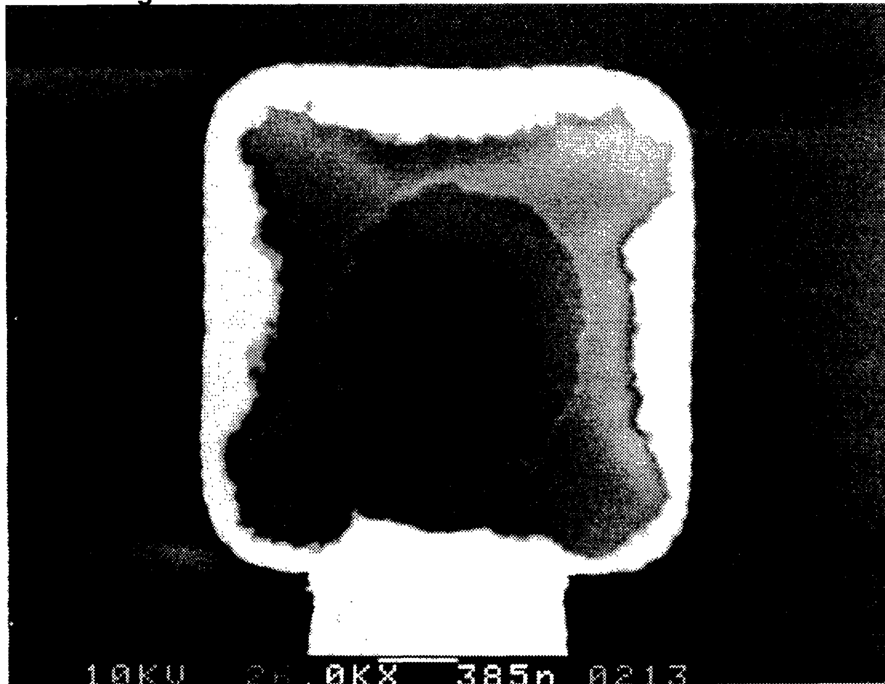

2. Integrity of the TiW Adhesion Layer:

Degradation of the patterned TiW adhesion layer was noted in scanning electron micrographs of the earlier 3.0μm high free-standing bridge structures. The typical appearance of a TiW via foundation is represented below in the S.E.M. micrograph of Figure 5. Since only the outer portion of the square feature seems intact, special scrutiny was given to the processes which occurred between the PSG contact etch and the tungsten deposition. During this phase of the fabrication process, a rounded-square hole was cut through the 5000Å of PSG to the underlying titanium-tungsten film. If the

wafer were to be exposed to a TiW etchant at this stage in the processing, the center of the titanium-tungsten square would be damaged first.

The established success of the PSG contact etch over titanium-tungsten films utilized in other microelectronic applications directed suspicions toward post etch treatment. A cleaning step that utilized a sulfuric acid solution was identified as the probable culprit, since sulfuric acid etches titanium-tungsten. In the development of the new fabrication process for the electrostatic deflection structures, the procedure which utilized the sulfuric acid clean was substituted for a more chemically benign resist strip.

Although the sulfuric acid solution appeared to be the cause of the unwanted etch of the titanium-tungsten film, another series of experiments was conducted in order to determine whether or not hydrofluoric acid would etch titanium-tungsten. This prospect arose from the knowledge that even though tungsten is fairly impervious, titanium is particularly susceptible to chemical attack from hydrofluoric acid. If the foundation layer was etched by HF, a new, isotropic PSG etchant would have to be utilized for the removal of the sacrificial glass. With these priorities in mind, three wafers with a 0.17µm film of silicon nitride were weighed, sputter deposited with 900Å TiW, reweighed, and mapped for sheet resistance using an automated four point probe system. The three wafer samples where then subjected to different etchant solutions: Pad Etch (1:1:1:: Acetic Acid: Ammonium Fluoride: Aluminum Acetate), BOE (Buffered Oxide Etch, which contains HF), and 10:1 HF. BOE and Pad Etch were selected for this experiment because, like 10:1 HF, these solutions also etch PSG glass, and thus could potentially be substituted for the hydrofluoric acid solution in the final fabrication sequence. The etch time used in each case was 1.5 minutes. Following removal from the etchant baths, the samples were vigorously rinsed in deionized water, blown dry, and baked for 15 minutes

at approximately 80°C. Following the dehydration, each sample was reweighed, and the sheet resistance remeasured. For all three of the samples, no significant weight loss or change in sheet resistance was evident. Since no difference in mass or thickness of the film was detected, titanium-tungsten was assumed to be sufficiently stable in hydrofluoric acid. As a result the hydrofluoric acid solution remained as the etchant for the final removal of the sacrificial glass.

3. Sample Preparation Prior to PSG Etch:

Experience from the processing of previous free-standing structures and initial etch experiments with the electrostatic deflection structures indicated that one failed device may not only physically destroy neighboring beams, but is also capable of producing hundreds of loose tungsten beams which can cause electrical shorts in intact geometries. Thus in order to improve the odds that one broken deflection structure would not render useless an entire wafer of die, one pre-PSG etch wafer was cut with a diamond saw into pieces with 4-6 die per section. These small wafer pieces were then mounted on three inch wafers with epoxy. The three inch wafers were scribed with letters for identification purposes and the die numbered in increasing order in the direction of the wafer flat. In this capacity, the three inch wafers provided a convenient means for handling individual die.

Although the use of the diamond saw applied additional mechanical stresses to the tungsten structures, the PSG film was present to reinforce the beams at this stage of the processing. Likewise, the increase in dust-like particulates from the cutting of the silicon wafer did not present any significant problems. Overall, the mounting of the small wafer pieces on three inch wafers proved an effective way to not only maximize the number of structures surviving the glass removal process, but also provided an efficient accounting system for individual samples.

IV. Electrical Test and Measurement

A. C-V Deflection Measurements

A nondestructive technique that can electrostatically induce measurable beam deflections would be a useful tool in the study of microfeature mechanical properties. Such a method holds several advantages over other techniques that permanently alter test samples. A deflection structure capable of repeated testing is not only economical, but also scientifically more attractive. The ability to retest structures presents an opportunity for in-depth exploration of elastic properties, analysis of possible fatigue behavior, and direct determination of yield stress. The goal of this series of electrical measurements was to obtain capacitance versus applied voltage curves for voltages less than those that would lead to irreversible stiction of the beam to the underlying electrode.

An optical microscope probe station in conjuncture with a Hewlett Packard 4284A Precision LCR Meter was utilized to perform and measure the capacitive response of the test structures to electrostatic deflection. Initial measurements were conducted to determine the significance of parasitic factors, to survey yield of successfully fabricated (i.e. open-circuit) devices, and to explore a non-destructive voltage range for the beam structures. Probe tip capacitance was measured to be on the order of nanofarads by placing two probes on a single contact pad and measuring the capacitance with the LCR meter. Application of 0.5 volts created a short-circuit in a previously open-circuited beam structure. The current path within the short-circuited device was not ascertained. However, due to the extremely low yield of usable structures, a voltage ramp from zero to 0.45 volts was determined as a "safe" range for testing.

Following the initial investigations, a procedure for deflection testing was implemented. Electromechanical testing of the free-standing tungsten air-bridge structures was conducted using a P.C. driven Hewlett Packard 4284A Precision LCR Meter and optical microscope apparatus. The electric potential was ramped in 100 discrete voltage steps from zero to 0.45 volts with a final capacitance measurement at zero volts. Using a 20 mV, 100kHz test signal, capacitance readings were collected after each voltage step. The time between a voltage increase and the corresponding capacitance measurement was a variable set by the user. Electrical contact to the test structure was accomplished by placing a probe tip on one of the two, long tungsten pads, and another probe on the square TiW electrode contact pad. Both the ramped DC voltage and the 0.20 mV AC signal were achieved through these electrical contacts.

The usefulness of C-V data from the electrostatic beam bending tests finds foundation in the model of the of the tungsten beam and titanium-tungsten film as the upper and lower plates of a capacitor. In a parallel plate capacitor, assuming negligible fringing and an air dielectric, the total capacitance of the structure is given by Eq. 1, which shows that capacitance is inversely proportional to the distance between the capacitor plates. Thus, deflection information may be obtained from changes in beam capacitance. Furthermore, the electrostatic force is a function of the applied voltage. Using the parallel plate assumptions, the electrostatic attraction can be calculated by [17]:

$$\vec{F} = \Sigma(q\,\vec{E}) = \frac{\varepsilon_0 A V^2}{d^2}, \qquad \text{(Eq. 2)}$$

where q is the charge on the plates; $\vec{E}$ is electric field; A is the beam area parallel to the electrode surface; and V is the applied voltage. The premise of C-V deflection

measurement is based on the fact that measured capacitance is a function of the gap distance and electrostatic force is a function of the applied voltage.

The assumptions of negligible fringing and purely elastic bending lead to equations such as that developed by Wang et al. [18]:

$$\frac{C^3 V^2}{(C-C_o)} = \frac{2\, d_o\, \varepsilon_o\, \sigma\, (1-\nu) w^2\, l\, t\, \mathbf{k}}{\frac{\mathbf{k}\, l}{4} - \tanh\left(\frac{\mathbf{k}\, l}{4}\right)}\ ;\ \mathbf{k} = \left[\frac{12\ \sigma\ (1-\nu)}{E\, t^2}\right] . \qquad \text{(Eq. 3)}$$

Here, E is the modulus of elasticity; w,t and l are the width, thickness and beam length, respectively; σ represents the biaxial film stress; Poisson's ratio is given by ν; d_o stands for the initial distance between the plates; and the initial capacitance is C_o. The above equation is simplified by the fact that the hyperbolic tangent goes to 1 for large, positive arguments. Therefore, the elastic modulus can readily be determined from C-V deflection data. The shortcoming of the simplified parallel plate approach is its incompatibility with realistic microfeature geometries in which fringing fields may make significant contributions to overall capacitance. Complications that arise from fringing of electric fields and charge redistribution will be discussed in the following section.

B. Determination of the Pull-in Voltage

A technique for determination of the elastic modulus of microbeam materials through potentially destructive testing has been developed by Osterberg et al., and will be reviewed in this section. [19] This procedure requires the collapse of the capacitor referred to as "pull-in." Although this snap-action of the beams toward the lower electrode is not necessarily a destructive technique, for a large number of materials and beam geometries such a test can only be executed a single time. Contacting of metal films

may cause welding, and test structures with large beam-to-electrode spacings may yield or fracture during pull-in.

Based on a strictly electrostatic model in combination with classical beam theory, this analytical approach is particularly attractive because capacitance is absent from the governing equations. Although derived in part through the assumption of an infinite parallel plate capacitor, this analysis directly depends on neither capacitance nor beam width. In fact the electrostatic force (Eq. 2) relates to the derivative of the capacitance (Eq. 1) in regard to the vertical gap distance. For this reason, the applied force may be considered less affected by the presence of fringing electric fields, and the model may be tentatively extended to investigate structures where fringing may be significant.

Pull-in occurs during electrostatic beam deflection when the applied electrostatic force can no longer be countered by the resolving force of the beam. For the purpose of determining these forces, a simplified model is constructed utilizing an effective spring constant as a lumped parameter description of the beam geometry and properties. [19] As depicted in Figure 6, the deflecting beam can be represented as capacitor with one plate fixed to a rigid constraint and the second plate suspended by a spring.

Figure 6. Effective Spring Constant Model

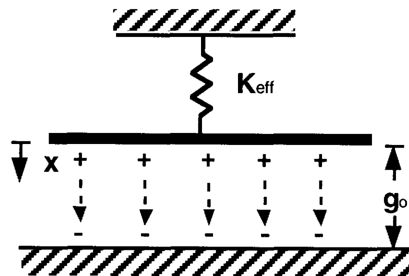

In the above illustration, g_o denotes the initial vertical spacing between the plates (i.e. beams and electrode film), and K_{eff} signifies the effective spring constant. Thus, the force (F_r) required to move the beam in the x direction is calculated by:

$$F_r = K_{eff}\ x. \qquad \text{(Eq. 4)}$$

As represented in Figure 6, x=0 at the initial beam-to-electrode distance. Similarly, the electrostatic force (F_e) is given by:

$$F_e = \frac{V^2 \varepsilon_o A}{2(g_o - x)^2}. \qquad \text{(Eq. 5)}$$

The term V represents the applied voltage; ε_o is the permittivity of free space; A is the area of the beams facing the electrode film; and the distances g_o and x are defined in Figure 6. The point of instability occurs when F_r and F_e are equivalent. The relationship between the forces is depicted in Figure 7. Three stable solutions are evident for the lowest of the F_e curves; these points are numbered. Obviously, point three is an unphysical solution since it occurs at a deflection greater than g_o, and point two will not be attained due the starting position at zero deflection. The instability labeled on the graph corresponds to the second voltage curve, where the voltage equals V_{pi}. As can be seen in this diagram, for voltages greater than V_{pi}, no solutions exist for $F_e = F_r$.

Figure 7. Instability in the Capacitor/Spring Model

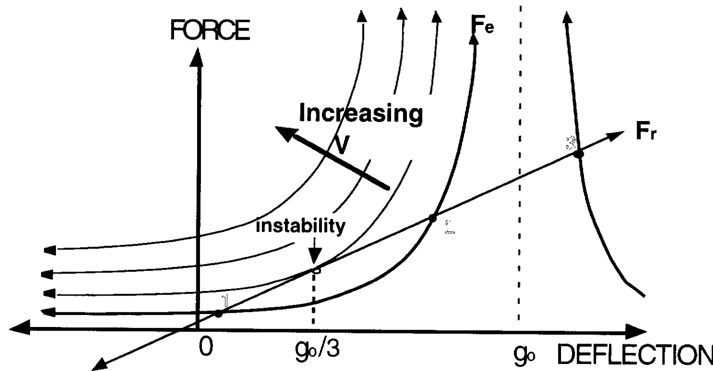

The value of the pull-in voltage, V_{pi} may be deduced by taking the derivative of the expression produced from the combination of Eq. 4 and Eq. 5, as shown below:

$$V_{p.i.} = \left[\frac{(g_o - x)^3 K_{eff}}{\varepsilon_o A}\right]^{\frac{1}{2}} . \quad \text{(Eq. 6)}$$

Furthermore, through rearrangement of the variables, the effective spring constant, K_{eff} can be expressed as:

$$K_{eff} = \frac{V^2 \varepsilon_o A}{(g_o - x)^3} . \quad \text{(Eq. 7)}$$

The spring constant represents the mechanical response of the beams to the applied electrostatic force, and can be equivalently derived through classical, elastic beam bending.

Figure 8. Beam Fixed at Two Ends

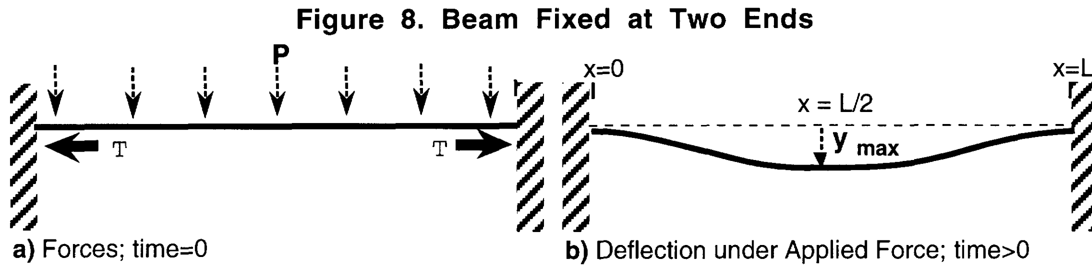

For the geometry of Figure 8, in which a beam under tensile stress is fully constrained at both ends and subjected to a constant load, the equation of motion is given as [20]:

$$EI\, y'''' + T\, y'' = w\, P. \quad \text{(Eq. 8)}$$

In this expression E is the elastic modulus; I represents the moment of inertia; P is the electrostatic pressure applied to the beam (given by $\vec{F}$ of Eq. 2 per area); and T refers to the intrinsic stress within the beam. Solving for the deflection y(x), and substituting x=L/2 obtains the following equation for the maximum deflection at the beam midpoint:

$$y_{max} = y\left(\frac{L}{2}\right) = \frac{wPL}{8\tau}\left[L + \frac{4\left(1 - \cosh\left[\sqrt{\frac{T}{EI}}\left(\frac{L}{2}\right)\right]\right)}{\sqrt{\frac{T}{EI}}\sinh\left[\sqrt{\frac{T}{EI}}\left(\frac{L}{2}\right)\right]}\right] . \quad \text{(Eq. 9)}$$

In turn, T and I are defined by:

$$T = w\, t\, \sigma(1-\nu) \quad \text{(Eq. 10)}$$

and

$$I = \frac{wt^3}{12}. \qquad \text{(Eq. 11)}$$

Above, σ is the biaxial film stress; t refers to the film thickness; and ν is Poisson's ratio. The effective spring constant can be found directly from the expression for the point of maximum beam bending through the relation:

$$y_{max} = \frac{P}{K_{eff}}. \qquad \text{(Eq. 12)}$$

The interdependence of the electrostatic pressure, the effective spring constant, and the maximum deflection leads to the following solution for the effective spring constant:

$$K_{eff} = \frac{8\,\sigma(1-\nu)\,t}{L^2\left[1 + \frac{2[1-\cosh(u)]}{u\,\sinh(u)}\right]}, \qquad \text{(Eq. 13)}$$

where

$$u = \frac{L}{2}\left[\frac{12\,\sigma(1-\nu)}{E\,t^2}\right]^{\frac{1}{2}}. \qquad \text{(Eq. 14)}$$

Once K_{eff} is determined, the pull in voltage can be tabulated through application of Eq. 6 from the suspended capacitor model of Figure 6. Through this method the value for the displacement, x at which the instability occurs is found to be $g_o/3$. Thus, from the combination of equations 6, 13 and 14 the expression for the pull-in voltage becomes [21]:

$$V_{p.i.} = \left[\frac{\gamma_1\,\sigma\,(1-\nu)t\,g_o^3}{\varepsilon_o\,L^2\left(1 + \frac{2[1-\cosh(\gamma_2\,u)]}{\gamma_2\,u\,\sinh(\gamma_2\,u)}\right)}\right]^{\frac{1}{2}}. \qquad \text{(Eq. 15)}$$

The terms γ_1=2.78, and γ_2=0.98 can be calculated directly from the equations or determined from finite element simulation data within an extremely close margin of agreement. In the above equality, u remains as defined in Eq. 14, and all other variables are previously described. In short, a description of pull-in is obtained that relates beam geometry and thin film mechanical properties to the voltage at which the electromechanical instability occurs. Therefore, pull-in voltage data can be utilized to

experimentally measure the intrinsic stress or elastic modulus of thin film bridge structures.

Measurement of the pull-in voltage was conducted through application of a DC bias to the beam test structures. A probe station/optical microscope assembly was utilized in order to obtain electrical contact to the bridge structures. Three probe tips were required for this series of tests. An analog DC power supply was used to produce the electrostatic force on the beams, and a digital voltmeter was also contacted to the beams using a second probe to measure the bias applied by the first contact pin. The third tip was placed on the pad of the underlying electrode film and connected to an ammeter. Figure 9 contains a schematic of the electrical testing apparatus.

Figure 9. Pull-in Voltage Apparatus

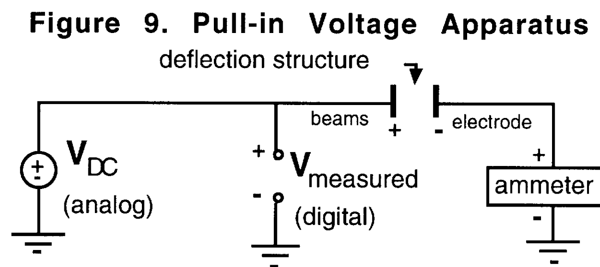

The digital voltmeter was necessary for accurate knowledge of the voltage applied by the analog power supply. Testing procedure required slow ramping of the DC bias from zero to the pull-in voltage. The voltage was increased by hand at a rate of approximately a tenth of a volt per 2 seconds. When the bias reached the maximum of the fine adjustment knob at 3.5 volts, the voltage was reduced to zero and the coarse adjustment was used to elevate the new starting potential to 3-3.5 volts. Additional bias increases utilized the fine adjustment capability of the power supply. The purpose of the ammeter was to determine the moment when the tungsten beams contacted the TiW film. Since pull-in coincides with an abrupt change in the conductivity of the tungsten-titanium-tungsten test structure, the ammeter was used to observe the short-circuit created upon collapse

of the beam-electrode capacitor. The means for direct observation of the pull-in was through visual verification using the optical microscope.

V. Results and Discussion

A. Process Results:

Free-standing tungsten bridge structures were successfully fabricated. However, yield was significantly affected by a variety of processing problems. The overall characteristics of the deflection structures produced will be presented with respect to processing parameters. In addition, the factors that reduced the number of useful deflection structures will be discussed in this section.

1. Over-etch of the TiW Film

A degree of nonlinearity was expected in the tungsten beams due to the step height at the edge of the 900Å TiW electrode film. However, the large protrusions evident on the beam undersides during preliminary inspection by scanning electron microscopy indicated that the actual step height had been altered at some point during the processing. The cross-sectional view of a device found in Figure 10 was generated to investigate the source of the apparent processing error. The cross-sectioned structure differs from the deflection structure due to the presence of via supports along the beam length. In the photo, the bright titanium-tungsten film is evident both under the beams and below the tungsten via plug (center). Of particular interest is the silicon nitride film directly below the TiW layer. Over-etch during the patterning of the titanium-tungsten electrode is evident in the regions to the right and left of the via support. The attack of the silicon nitride film increased the effective step height of the patterned electrode film

by a factor of approximately three times the intended dimensions. The enhanced topography of the wafer surface intensifies step coverage problems during the later depositions of the phosphosilicate glass and the tungsten. Also evident in the cross-sectional view are voids within the tungsten beams; these defects, which weaken the overall structural integrity of the beam, might have been avoided had the silicon nitride film remained unetched.

Figure 10. Via Cross-Section Showing Etch of Silicon Nitride Underlayer

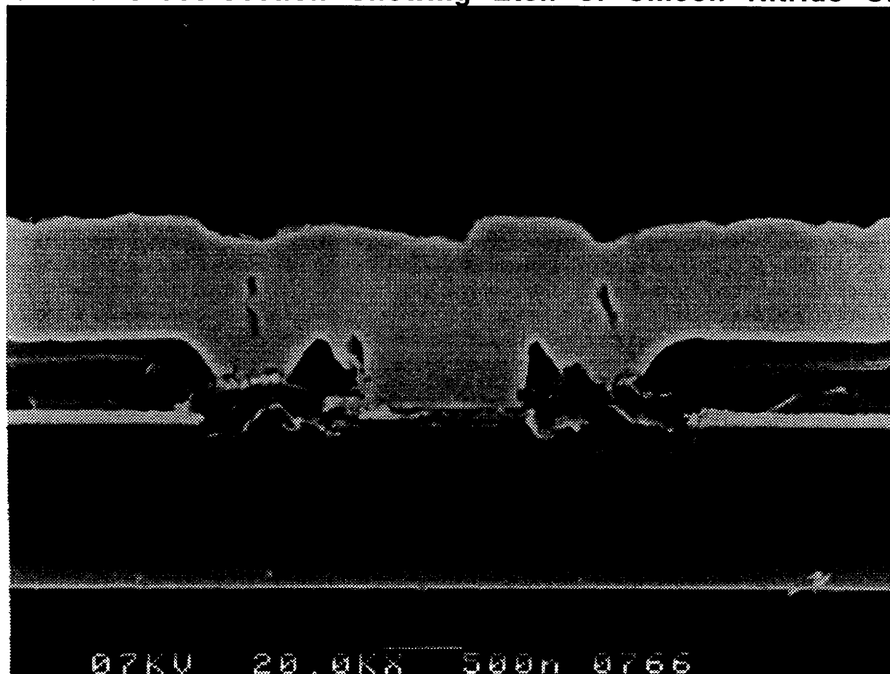

2. Photoresist Residue:

Following the 400°C deposition of the CVD phosphosilicate glass, thin features that initially appeared to be cracks in the glass film were observed through optical microscopy. Closer inspection revealed that the threads corresponded in length and general orientation with the geometries of the titanium-tungsten foundation/ground electrode layer. These "stringers" were lines of photoresist residue that had remained stuck to the side walls of the titanium-tungsten features and were subsequently trapped

below the phosphosilicate glass film. The entire fabrication sequence was completed for these samples. No noticeable effects, other than the thin dark lines, were evident when viewing the structures by optical microscopy. Potential complications introduced by this processing problem include deformation of the glass film due to deposition over residual matter, and possible electrical shorting within the deflection structures due to conductive threads of the burnt polymer.

Figure 11. Tungsten Beams with Photoresist Residue

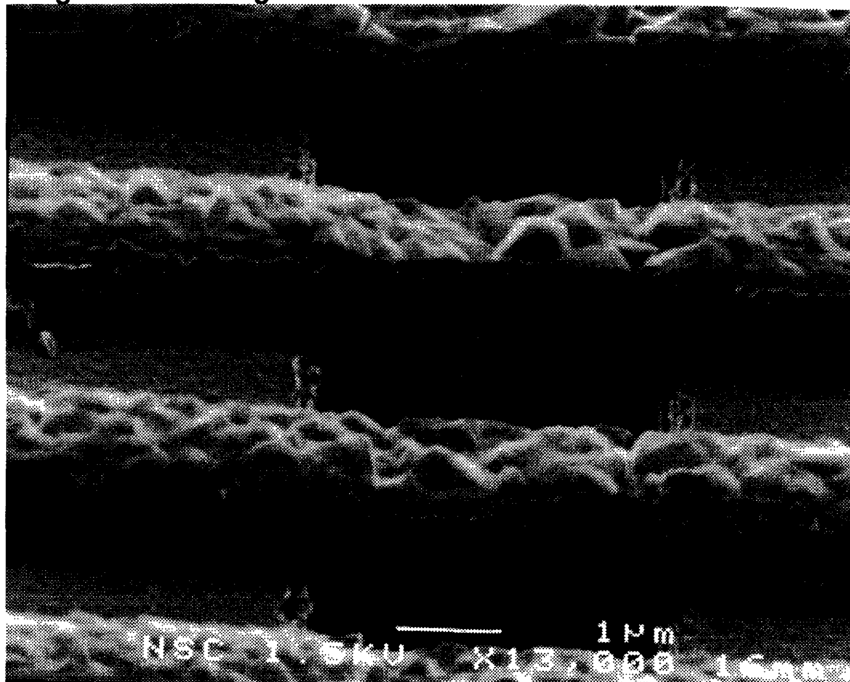

The resist residue had formed due to an inadequate photoresist removal process, which consisted of two asher cleans and a rinse in deionized water. Although this photoresist removal process had on earlier structures successfully replaced the more conventional, sulfuric acid solution resist strip, the larger features of the deflection structure layout evidently require a more thorough cleaning technique. A similar problem was encountered following the PSG removal from the first fully-processed etch rate samples. Visual inspection using a scanning electron microscope revealed the presence of excessive residual matter hanging from the deflection structure beams.

Figure 11 is an electron micrograph of the appearance of these ash-covered beams. Prior to the removal of the sacrificial glass, a one hour 80°C solvent clean (n-methyl pyrolidone and ethanol) successfully removed the resist residue left by the final lithography step for all later samples.

Figure 12. Nodules on Tungsten Beams

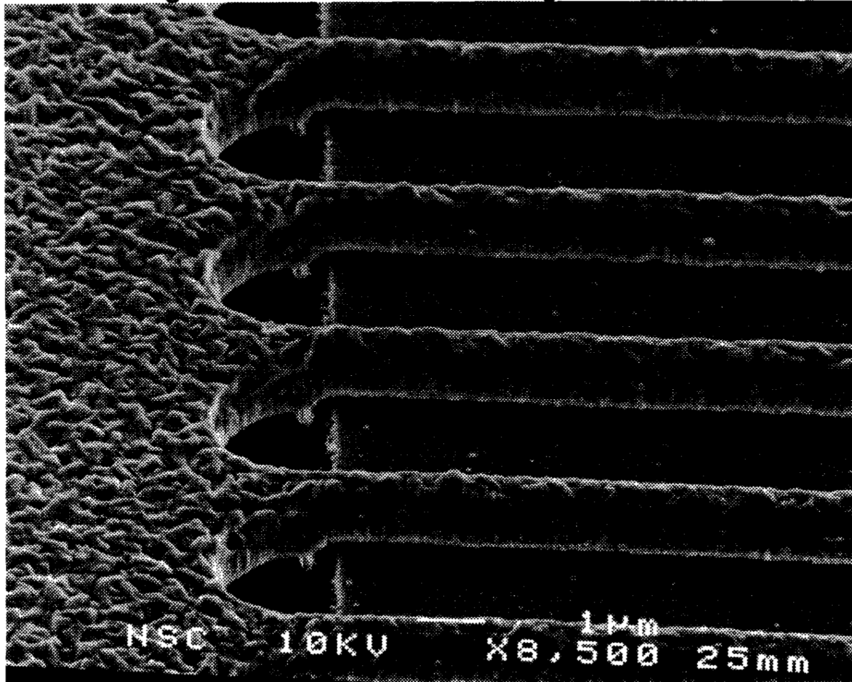

3. PSG Step Coverage

As evident in Figure 12, tungsten spikes exist on most of the beams of the electrostatic deflection structures. This feature was formed when chemically vapor deposited tungsten filled a seam along the PSG glass surface. The crevice in the PSG film was formed when the growth of CVD phosphosilicate glass from the titanium-tungsten side wall and the silicon nitride surface met along a diagonal crease and failed to fuse together. Figure 13 illustrates the formation of the PSG crack and the cusp of the tungsten line. In the diagram, the series on the right indicates the compounded shape effects caused by the etched silicon nitride substrate film and the step coverage

difficulties of the deposited CVD glass, while the sequence on the left represents the intended processing results.

Figure 13. Step Coverage Effects

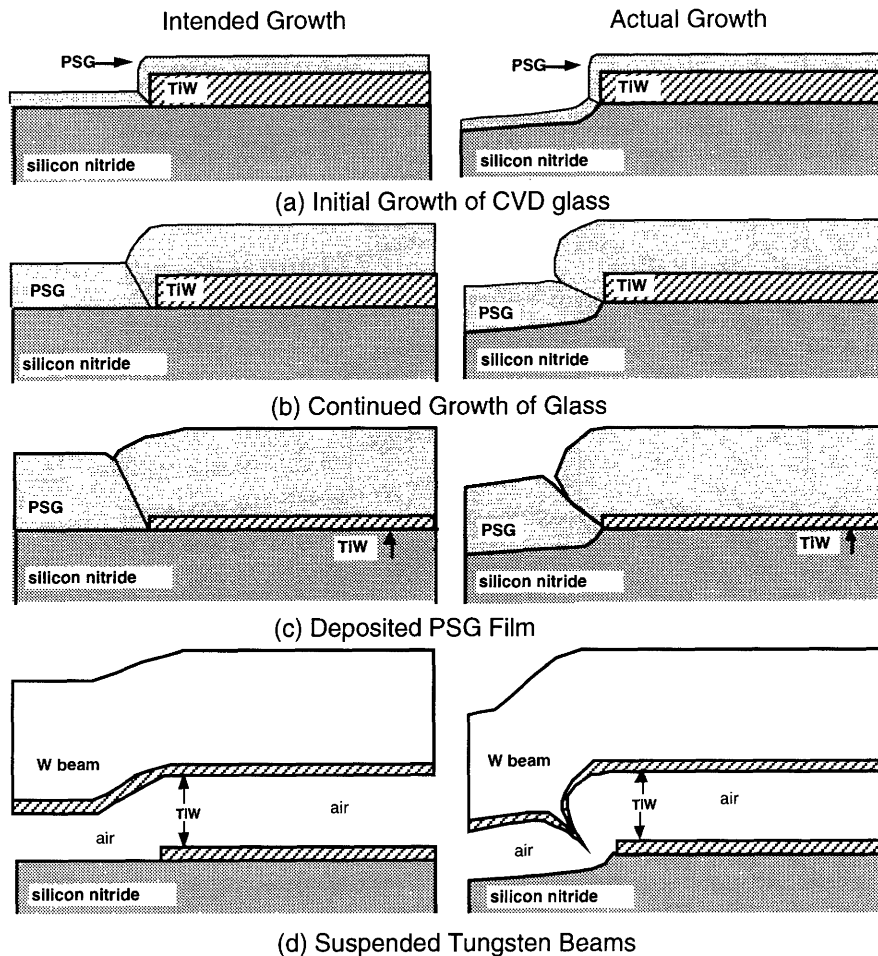

(a) Initial Growth of CVD glass

(b) Continued Growth of Glass

(c) Deposited PSG Film

(d) Suspended Tungsten Beams

The presence of these tungsten cusps on the beams is particularly disturbing due to the close proximity of the spikes to the titanium-tungsten electrode film. The most obvious impact of these features was electrical shorting of the beams directly to the ground electrode. Fortunately, the PSG crease, although omnipresent, varied in depth across the surface of each wafer. As a result, the size of the tungsten spikes varied from one location to another. Scanning electron micrographs of the deflection structures are found in Figure 12 and Figure 14. In these images, many of the beam stalactites contact

the TiW electrode, while other samples merely have small tungsten nodules along their underside.

Figure 14. Beam Shorted to Ground by Tungsten Cusp

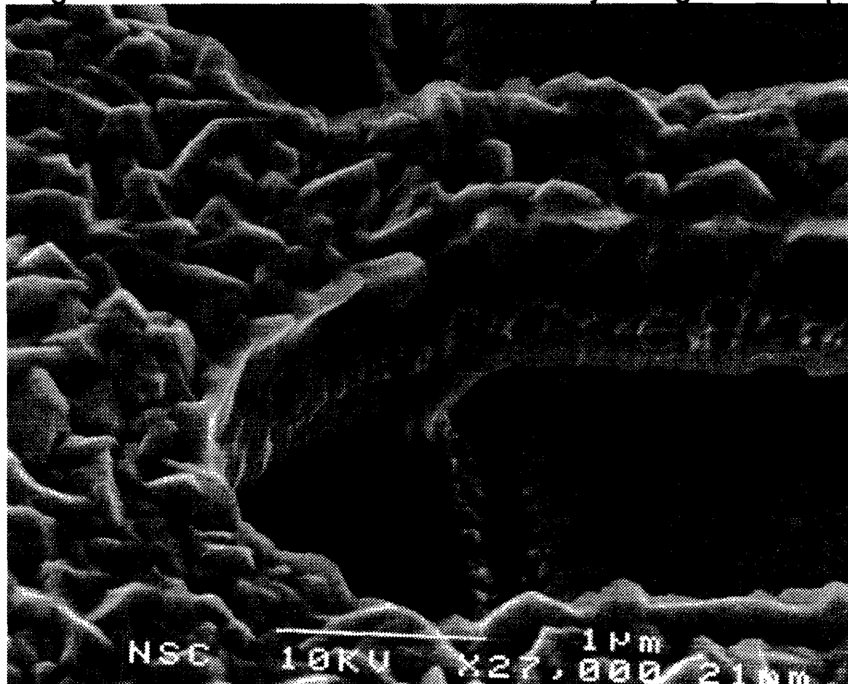

4. Etch of Sacrificial PSG Film:

Investigation of the PSG etch in 10:1 HF indicated an etch rate of approximately 5000Å/min. for a continuous film, and questionable results for a film under patterned tungsten between 3-4000Å/min. Previous attempts to determine a precise etch time having failed, the samples mounted on three inch wafers were subjected to a range of etch times. The samples and their corresponding etch times were as follows:

PSG Etch of Prepared Samples

Sample I.D.	Etch Time (min:sec)
A-Z	1:00
AA-AH	1:15
AI-AM	1:30
AN-AR	1:45
AS-AW	2:00
AX-BA	2:15

Structures completely clear of phosphosilicate glass were found at etch times of 1:15 seconds. On the other hand, some die subjected to over two minutes in the hydrofluoric

acid solution contained structures with significant areas of glass cover. The wide variation among the etch results, and absence of any correlation with the etch time indicates a strong dependence on uncontrolled process parameters. Factors such as the flow within the HF bath or the temperature may have had significant effects on the etch rate. Nonetheless, freestanding tungsten air-bridges were successfully fabricated on samples with etch times ranging from 1 minute and 15 seconds to 2 minutes and 15 seconds.

Figure 15. Detached Via & Preferential Etch of PSG Around TiW Features

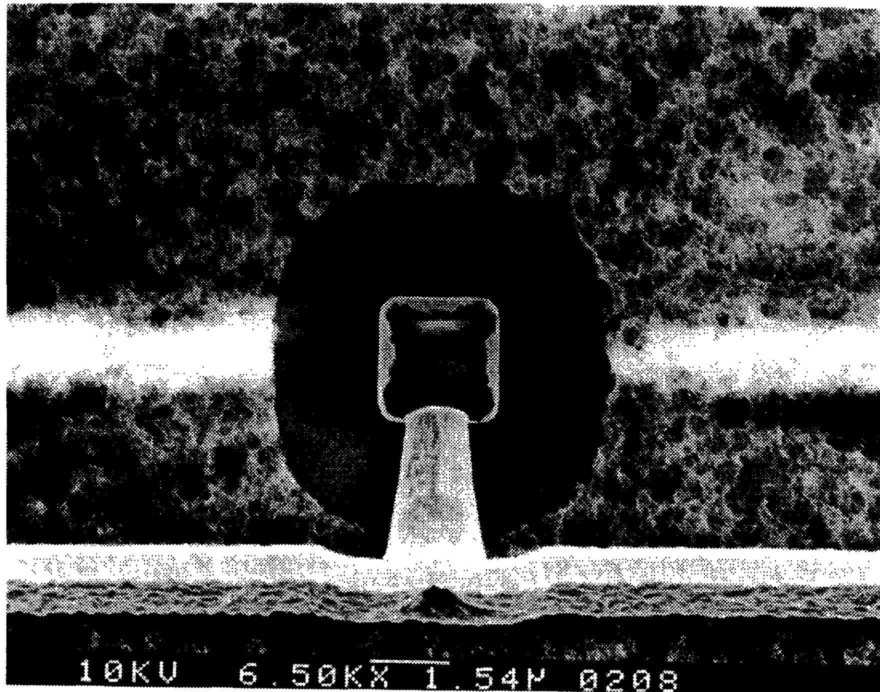

Another point of interest in regard to the etch of the phosphosilicate glass is the increased etch rate in the areas immediately adjacent to the titanium-tungsten foundations. S.E.M. analysis reveals this preferential etching to be a reoccurring effect. Insufficiently etched samples from the earlier crosstalk measurement structures, as well as the deflection structures commonly exhibit a partially etched glass field with circles of complete clearing centered around the TiW features. Figure 15 and Figure 16 are scanning micrographs exhibiting this effect. Whether the etch rate is enhanced for electrical reasons having to do with proximity to conducting material, or whether a

more complicated chemistry involving reaction of HF and TiW facilitates the removal of the glass was not determined in this study.

Figure 16. Attached Corner Via & Preferential Etch of PSG Around TiW

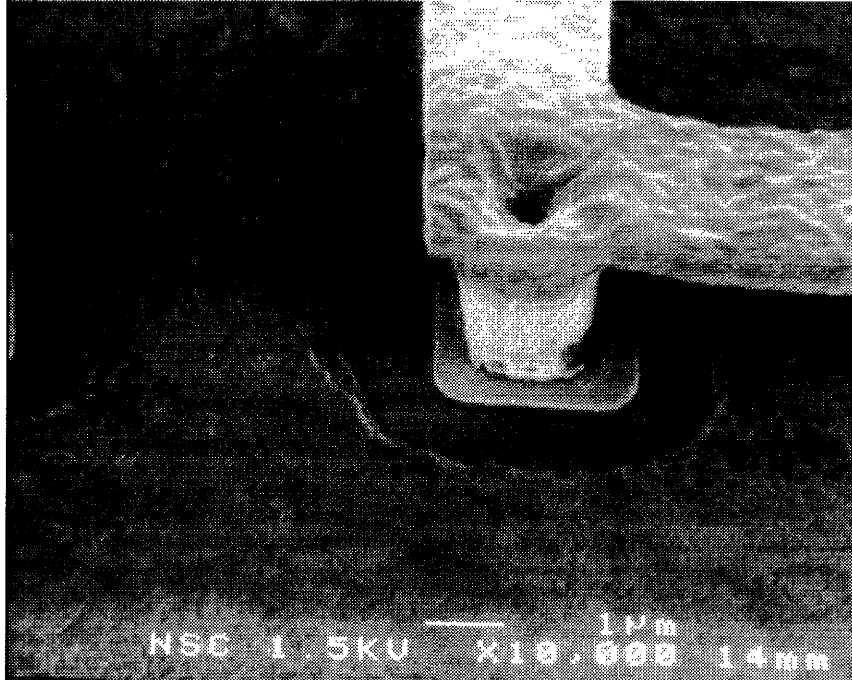

Beam breakage during the PSG etch process greatly reduced yield. The 1μm wide deflection structures proved particularly fragile, while damage among 1.5μm wide beam structures was significantly less common. While extreme care was taken to lessen the forces upon the wafer surface during the etch process catastrophic failures were present in 75% of the sample die. Future work in this area must overcome the brutality of the PSG removal process. Development of a reliable gas phase etch or the use of surfactants within the etchant solution to lower surface tension are possible avenues for continued investigation.

5. The Tungsten Film

The beams were formed from a one micron thick chemical vapor deposition (CVD) of tungsten from WF_6 at 400°C (approximately 0.12 T_{melt}) in a warm-walled reactor, and thus growth occurred within a mass transport limited regime. The resulting tungsten film can be viewed in Figures 12,14, and 17. The tooth-like,

columnar grain structure evident in Figure 14 and schematically represented below in Figure 18 agrees with grain structure predictions for CVD processes in which the deposition temperature is less an 0.3 times the melting temperature. [22]

Figure 17. Damage to TiW Film Following PSG Etch

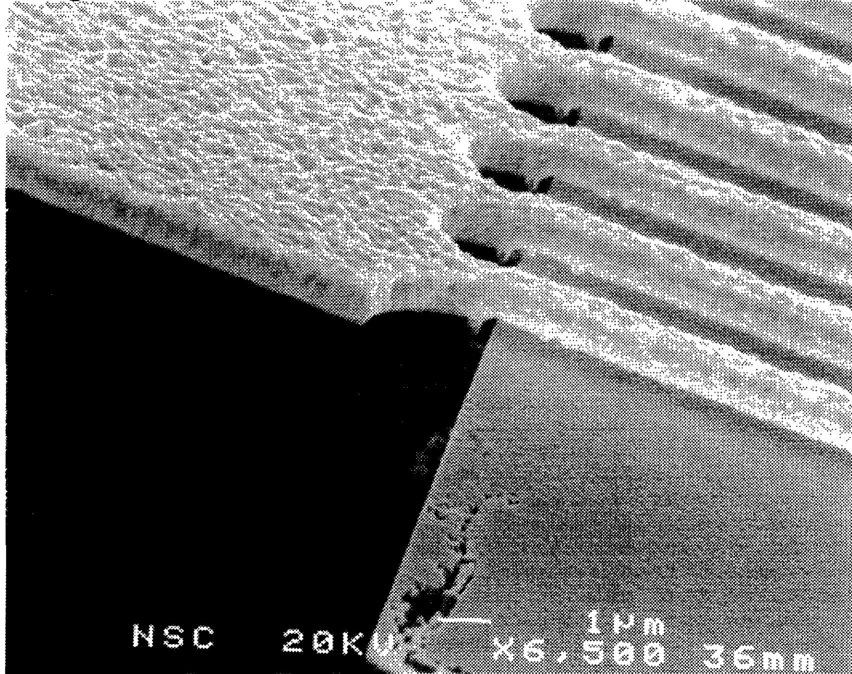

Figure 18. Columnar Grain Structure

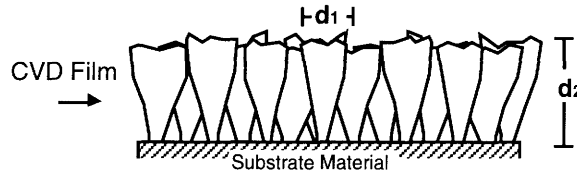

In such a grain structure the grain dimensions in the plane of the film (d_1) are generally much smaller than the vertical heights of the grains (d_2), which are on the order of the film thickness. The electron micrographs reveal obvious surface roughness on the order of a quarter micron; this topography is directly related to the grain structure and provides a fair estimate of the grain dimensions in the plane of the film. Although, (200) texture of a CVD tungsten film deposited on a thin layer of sputtered tungsten (rather than sputtered TiW) has been reported in the literature, [23] determination of the crystallographic texture of the tungsten deflection structures was

not conducted. The lack of textural characterization of the tungsten beams, however, is not a highly critical factor in this case, since tungsten exhibits only weak anisotropy in its elastic behavior. [24]

The tungsten film was deposited in a state of tensile stress. The built-in stresses of the thin film are due largely to two distinct sources: 1) thermoelastic stresses that arise due to mismatch of the film and substrate thermal expansion characteristics, and 2) intrinsic growth stresses that are directly related to the film microstructure in regard to grain size, crystalline defects, and texture. [23] Approximation of the thermoelastic stress within the tungsten film can be easily calculated from the expression [25]:

$$\sigma_{th} = (\alpha_f - \alpha_s) \frac{E_f}{(1 - \nu_f)} (T_{dep} - T) , \quad \text{(Eq. 16)}$$

where σ_{th} is the thermoelastic stress; α_f and α_s represent the thermal expansion coefficients of the film and substrate respectively; the elastic modulus of the thin film is given by E_f; and $(T_{dep} - T)$ describes the temperature change from the deposition reactor to the final environment. Assuming the thermal expansion coefficients for tungsten and silicon to be approximately 4.5×10^{-6} °C^{-1} and 2.7×10^{-6} °C^{-1} respectively (values taken from the 67th ed. CRC Handbook), and utilizing a typical elastic modulus for tungsten of roughly 350 GPa, the film stress due to thermal expansion for the 400°C deposition process is calculated to be on the order of 320 MPa.

The overall film stress for the tungsten deposition process was monitored by the manufacturing facility to lie within a range of 700-900 MPa. Values for the film stresses were obtained through measurement of the substrate wafer curvature before and after the growth of the tungsten thin film. The wafer curvature technique, which

requires knowledge of neither the film elastic properties nor texture, utilizes the following relationship [26]:

$$\sigma_f = \frac{E_s\, t_s^2}{6(1 - \nu)\, t_f\, R} \qquad \text{(Eq. 17)}$$

to determine the overall stress within the film (σ_f), from the silicon wafer elastic modulus (E_s), the substrate thickness (t_s), the film thickness (t_f), and the radius of curvature of the wafer (R). The fact that stress measurements were not conducted for the actual wafers used in the fabrication of the deflection structures is unfortunate, especially since imprecise knowledge of the film stress limits the accuracy of deflection and pull-in data. However, for the purposes of demonstrating the feasibility of electrostatic beam bending characterization methods, the 700-900 MPa range offers at least general quantitative insight.

The biaxial film stress measured from wafer curvature analysis is the sum of the thermoelastic stress and growth stresses. The remaining 380-580 MPa tensile stress is regarded as the growth stress. The origins of this so called intrinsic stress has been the topic of some controversy. In general, growth stresses in polycrystalline films are attributed to the combined effects of surface tension, substrate bonding forces, crystallite boundary relaxation, and possible post-deposition phase transformations. [27] The growth regime, determined by the WF_6 and Ar gas flows and temperature during the deposition process, is the primary influence on the nature of the intrinsic growth stresses. Assuming the initial polycrystalline film forms from the nucleation of hemispherical islands that grow until they coalesce and take on cylindrical shapes, the balancing of the crystallite surface tension, substrate forces, and attraction between island surfaces leads to a built-in tensile stress. In addition, any changes in film density occurring after the bonding of the thin film material to the substrate, such as that experienced during phase transformation, also induce crystalline strain, and

therefore built-in stress. [7] The columnar grain structure, grain size, and crystallinity are all factors in the generation of the film stress state. Nucleation of microcracks or further heat treatment for reduction of intergrain tension could potentially, partially relax this stress. However, for the purposes of this investigation, the beams were subjected to no further heat treatments.

6. Appearance of Titanium-Tungsten Film

The titanium-tungsten via foundations as well as areas of the large TiW electrodes were visibly attacked. An S.E.M. micrograph of the typical damage to the TiW film can be found in Figure 17. The regions of TiW damage are not merely limited to the areas opened by the third masking step, which means that the film is subjected to the hostile chemical environment either before the PSG deposition or after the PSG removal. In addition, the titanium-tungsten is most attacked in the area where the PSG film first clears, i.e. around the vias and around the edges of the large electrodes. These observations indicate that the experiment which verified that HF does not etch titanium-tungsten may have been incorrect. Future efforts should explore an alternative PSG etchant that will not attack the titanium-tungsten features.

B. Electrostatic Deflection Results:

Initial survey of the fully processed samples revealed an extremely low number of unshorted beam structures. These electrical findings were visually corroborated by the tungsten cusps evident in Figure 12 and Figure 14. In spite of the process short-comings, a sufficient quantity of open-circuited beam structures were obtained for electrostatic deflection testing.

The initial capacitance of the 1.5μm wide deflection structures varied between 35-70pF, a value much greater than the predicted 28pF. Variations in initial capacitance between otherwise identical structures was strongly correlated with the relative sizes of the tungsten cusps and other beam defects. The spikes and large block-like nodules on the tungsten beams, which resulted from the increased step height at the electrode film edge, were probably the primary source responsible for the heightened capacitances.

1. Voltage-Capacitance Curves

The purpose of the this series of measurements was to observe and potentially measure beam deflections through changes in the overall capacitance of the multibeam structures. The design of the deflection structures was originally intended to produce data that could be used in an analysis similar to the one presented in Eq.3. Although such an approach would have had to correct for the capacitance contributed by fringing, calculation of the elastic properties from C-V data was numerically possible. Unfortunately, the heavily distorted beams produced through this faulty fabrication process greatly frustrated any useful quantitative measurement of the elastic properties from the collected data.

The electrostatic deflection program, which ramped a DC bias from zero to 0.45 volts and concluded with a measurement at zero applied bias, was extensively used on the deflection structures with 1.5μm beam widths; data from 110 individual tests using the C-V measurement program were compiled. While the initial capacitance was uniquely altered for each test structure, changes in capacitance were found to occur similarly with applied voltage for various samples. In all cases, capacitance changes on the order of 3.5-5.5 pF were attained and the capacitance returned to the initial value upon removal of the DC bias. The strong agreement between the initial and final data points throughout the tests indicated that in general the elastic limits of the tungsten film were

not exceeded by the forces applied. In addition, the similar capacitive response (i.e. ΔC) to applied electrostatic force observed for all samples demonstrated that the cusps and other processing artifacts at the beam ends did not greatly affect the deflection of these high aspect ratio beams.

Typical curves produced from the C-V deflection program can be found in Figure 19 and Figure 20. Perhaps the most interesting aspect of the data obtained from this series of tests was the apparent degradation of the beams upon repeated testing. Both graphs contain data from ten sequential repetitions of the C-V program. The center points represent the mean values for the capacitance measurements at each voltage and the bars represent ± one standard deviation of the data. While Figure 19 represents the results from the first ten deflection tests executed on Sample AL,1B, Figure 20 depicts the analogous data from test numbers forty through fifty of the same test structure.

Figure 19. Capacitance vs. Applied Voltage

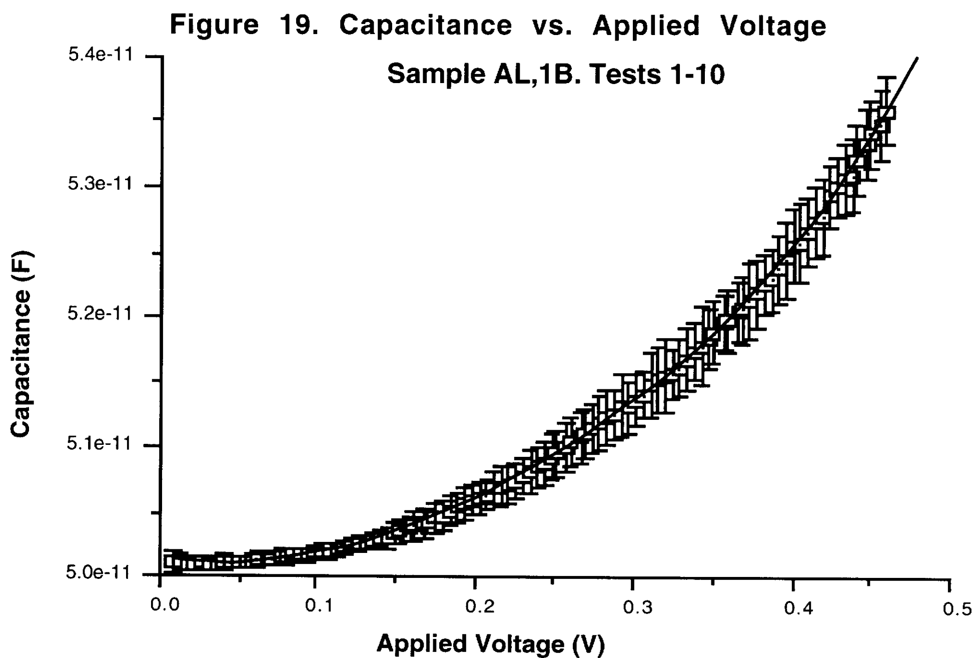

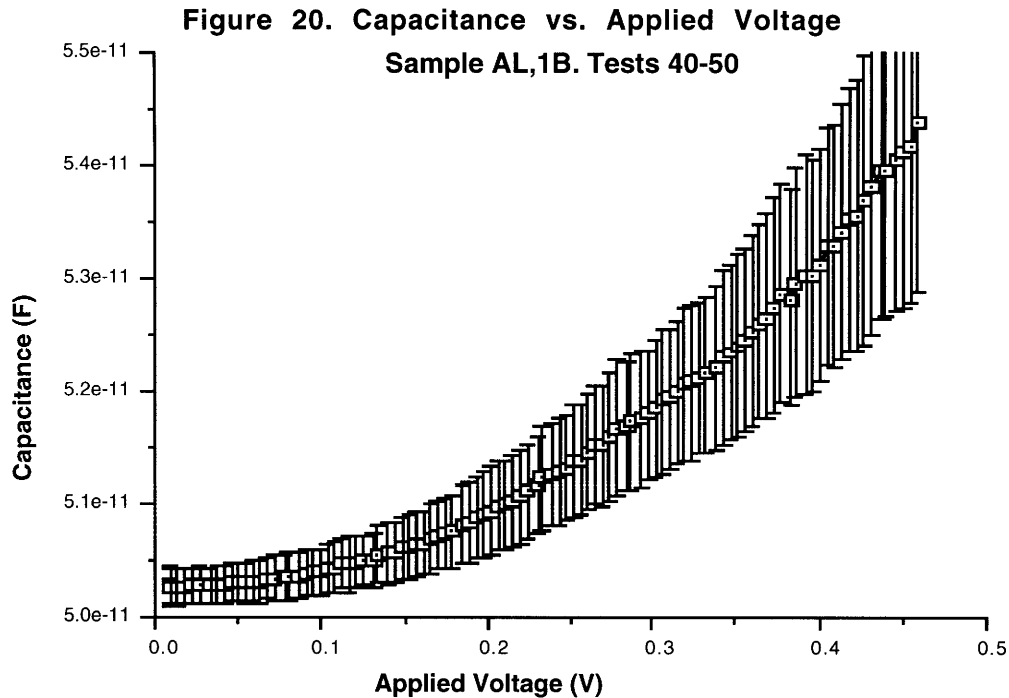

The standard deviations in the later data were approximately four times those of the initial findings. In addition, the initial capacitance and maximum capacitance were increased in the later tests. A possible mechanism for this alteration in the bending characteristics of the microbeams might be partial relaxation of the film intrinsic stresses with repeated bending; the nucleation of microcracks would lessen the built-in, tensile stress of the tungsten film and therefore allow larger deflections to occur as well as induce greater response variation (ΔC) among the individual beams. Grain boundary creep and other means of plastic flow in polycrystalline films also require consideration. Further investigation is necessary for identification of the actual mechanism responsible for the apparent microstructural change the tungsten film.

The C-V program developed in this study provided curves representative of the induced beam deflections. The ΔC results produced from the ramped voltage program proved highly smooth and quite repeatable for initial tests. Although processing difficulties created a large degree of initial capacitance nonuniformity among the

structures and frustrated any possibility for the extrapolation of deflection information, the progression of fatigue mechanisms in the microbeams may be monitored through this highly sensitive measurement scheme. Both the processing complications and electric field fringing issues experienced by this design could be greatly reduced in future structures by increased vertical gap distance. Accurate measurement of microbeam mechanical properties through electrostatic beam bending experiments was not demonstrated due to the highly flawed nature of the beam structures. Design improvements, such as a larger beam-to-electrode gap and increased beam width, hold promise for future electromechanical structures capable of reliable, quantitative determination of microbeam mechanical properties using this nondestructive technique.

2. The Pull-in Voltage

Although the deflection structures were not initially designed with the pull-in technique in mind, this analytical approach was particularly attractive since the deflection at the pull-in voltage is determined by the point of instability discussed in the previous section of this thesis, and not by capacitance measurement. The sample requirement for pull-in analysis is generally considered to be a beam width to vertical gap (w/g_o) ratio greater than 3. The deflection structures with 1.0μm and 1.5μm wide beams had w/g_o ratios of exactly 2 and 3 respectively, thus the test structures push the assumed limit of the model. For this reason, measurement of the pull-in voltage for these high aspect ratio/small gap structures was a particular point of interest.

Six beam structures were subjected to the destructive pull-in process. The video tape accompanying this paper contains footage of the elastic deflection and eventual pull-in of sample AH,4B. The table in Appendix B catalogs the applied voltages with regard to the video length. Of the six samples tested, two were 1.5μm wide beam structures and the other four were 1.0μm wide bridges. According to the model, the

structures differing in beam widths were expected to demonstrate the same pull-in voltage since Eq. 15 is independent of width. Considering the smaller w/g_o ratio of the 1.0μm wide beam structures, the bounds of the theoretical argument were significantly extended by these structures.

Since both the tungsten beams and titanium-tungsten electrode are highly conductive materials, a drastic increase in the current passed through the circuit was anticipated to coincide with the collapse of the capacitor. The short-circuiting effect was observed for only sample AH,4B. Although some question existed concerning the quality of the ammeter utilized in this experiment, the presence of a thin layer of the PSG glass may also have hindered good contact for the collapsed beams of the other structures.

Nonetheless, unmistakable pull-in was observed visually for all six deflection structures. The samples and the corresponding pull-in voltages were:

Sample I.D.	Pull-in Voltage (volts)
AH,4B	4.6 ± 0.2
AJ,1A	4.9 ± 0.1
AJ,3A	5.0 ± 0.2
AJ,1B	4.8 ± 0.2
AM,4A	4.4 ± 0.2
BP,5A	4.6 ± 0.1

Working within the limits of the testing equipment presented the most significant challenge of this procedure. The large errors associated with the reported pull-in voltages resulted from difficulties experienced in obtaining gradual increases in the applied voltage. While the digital voltmeter made possible immediate knowledge of the applied potential, increases in the voltage were sometimes much larger than intended, due to poor, manual control of the analog power supply. In addition to the problem with the applied bias, determination of the pull-in voltage required observation of the structure under the optical microscope, as well as simultaneous monitoring of the power supply, voltmeter, and ammeter. A digital power supply capable of automatic ramping,

and a curve tracer for determining the I-V characteristics of the deflection structure would have greatly improved the accuracy of this testing method.

From the calculation outlined in the previous chapter, Eq. 14 and Eq. 15 relate the pull-in voltage to the elastic modulus (E) and the film stress (σ). Since a range (700-900 MPa) rather than an exact measure of the film stress was obtained for the tungsten film used in these experiments, precise determination of the elastic modulus is not possible. Figure 21 is a graph of the elastic modulus vs. pull-in voltage for a tensile stress of 772.4 MPa, which is the biaxial stress at which the average measured pull-in voltage (4.71 volts) gives the bulk tungsten elastic modulus of 350 GPa. [6] Since all previous research indicates that the elastic modulus of a 1μm-thick film should be very close to that of the bulk, 772.4 MPa is most likely an accurate estimate of the biaxial stress of the film.

Figure 21. Elastic Modulus vs. Pull-in Voltage for σ = 772.4 MPa

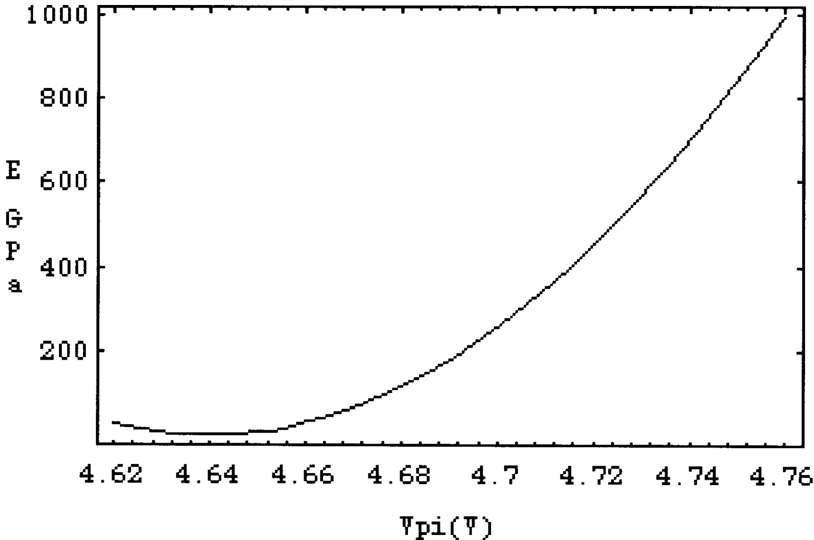

Due to the geometry of the test structures, calculation of the elastic modulus from the pull-in voltage is extremely sensitive to the stress within the beam. A three dimensional plot of the relationship described in Eq. 15 can be found on the left of Figure 22. The vertical axis represents the elastic modulus, while the two horizontal axes are the pull-in voltage (V_{pi}) and the biaxial film stress (σ).

Figure 22. Plots of Equation 15

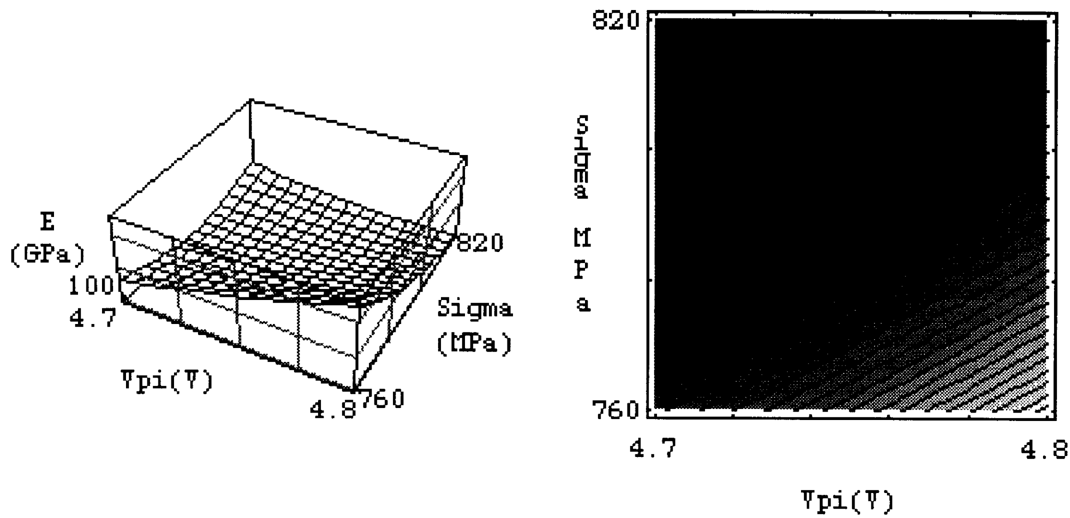

On the right of Figure 22 is a top view of the three dimensional plot. The shaded regions are contour lines for different values of the elastic modulus. The dark diagonal stripe toward the top right of the plot contains the modulus values expected for tungsten elasticity. Together, these figures depict the strong dependence of the measured elastic modulus on the stress state of the beam. Using the bulk elastic modulus and values from the top, middle, and bottom of the tensile stress range, the pull-in voltage of the deflection structures would be as follows:

σ (MPa)	V_{pi} (volts)
900	5.08
800	4.79
700	4.48

Although it is unfortunate that the exact tensile stresses of the test structure films were not measured and that the accuracy of the pull-in voltage measurement was poor, the recorded pull-in potentials are within the proper range, given tensile stresses of 700-900 MPa.

VI. Conclusions and Future Work

The free-standing tungsten bridge structures fabricated through the process sequence described in this thesis suffered from unforeseen processing errors and nonuniformities within the PSG step coverage and removal. The presence of tungsten cusps along the beam undersides, deterioration of the titanium-tungsten electrode film, and catastrophic structural failures during the liquid phase PSG etch were common problems encountered during fabrication. Although the final yield of intact structures was low, several were produced with only minor shape defects near the beam terminations. The tungsten microbeams were characterized by a columnar grain structure, surface roughness on the order of 0.25μm, and a film stress within the range of 700-900 MPa.

Direct interpretation of the film mechanical properties from deflection capacitance vs. voltage data was thwarted by the varied shapes of the tungsten beam defects and the complexities associated with the fringing field contributions of the misshapen beams. Improvements in the process sequence and variations in the design dimensions, such as increased beam-to-electrode distance and beam width, would raise the likelihood of reliable results for future efforts. The C-V deflection measurement system utilized in these experiments indicated possible stress relaxation within the tungsten film upon repeated bending. The ability to monitor small deflections through capacitance measurements may prove a useful technique in the investigation of the yield and fatigue behaviors of microdevice materials.

The technique of beam "pull-in" was successfully executed and provided realistic values for the elastic modulus within the range of film tensile stresses provided. Exact

knowledge of the film stress and more precise determination of the pull-in voltage could be easily incorporated to improve the accuracy of this characterization method. In addition, structures of differing lengths should be included in future experimental designs, since beam length rather than width determines the force coinciding with the pull-in instability. If the film stress was indeed around 772 MPa, the apparent accuracy of this technique indicates that the model can be extended for the study of beam geometries with w/g_0 ratios as low as 2. Successful application of the model to higher aspect ratio structures would reinforce a theory that, since electrostatic force is less affected by reduced gap dimensions than capacitance, the actual limitations of the pull-in model lie well below the conservative estimate of $w/g_0 > 3$. Although a destructive test for many materials, the pull-in voltage calculation provides an elegant solution to the determination of thin film elastic properties and is applicable to a wide range of microfeature geometries.

The promise and difficulties associated with the utilization of surface micromachining technologies and electrostatic force as means for the study of microfeature mechanical behavior have been explored in this project. With improvements in deflection structure processing and design, nondestructive C-V deflection testing may become a reliable tool for the study of microbeam (and thin film) elastic and plastic behavior. The destructive "pull-in" technique holds much promise for the measurement of microbeam (and thin film) elastic moduli, provided film stresses are precisely characterized and reliable electrical test instruments are used. In conclusion, the application of electrostatic force to surface micromachined test structures has been shown to offer multiple opportunities for investigation of the mechanical properties of thin films and thin film microfeatures.

Appendix A: Video Tape Voltage Index

This section describes the voltage history experienced by Sample AH,4B as recorded on the accompanying video tape. The table below contains the values of the applied DC bias in regard to the playing time.

Tape Counter	Applied Bias (volts)
0:47	0
0:47-1:10	ramped 0 - 1.9
1:10-1:15	held 1.9
1:15 -1:23	ramped 1.9 - 2.7
1:23-1:27	held 2.7
1:27-1:43	ramped 2.7-3.5
1:43-1:48	held 3.9
1:48-1:49	0
1:49-1:58	ramped 3.9
1:58-2:04 (pull-in)	ramped 3.9-4.6 (±0.2)
2:04-2:14	varied 4.6-0, 0-5

The bias was removed at 1:01 because the maximum of the fine adjustment knob of the power supply had been attained. The voltage was then turned off. The beams returned to the original green color, thus indicating that the previous bending had been within the elastic limits of the material. The coarse adjustment knob was then used to quickly raise the voltage to approximately 3.5 V and the fine adjustment was utilized for further ramping of the voltage. The sudden color change from pink to green at 2:04 was the pull-in of the beams corresponding to the applied bias of approximately 4.6 volts. The electrical shorting of the structure measured by the ammeter corroborated that instability had occurred. Subsequent changes in the voltage produced neither visible changes in the appearance nor the conductivity of the structure.

References

[1] R. W. Hoffman. Physics of Thin Films, **3**. G. Hass and R. E. Thun (editors), Acedemic Press: New York, 1966. p. 218.

[2] A. Catlin and W. P. Walker. *Journal of Applied Physics*, **31**, 1960. p. 2135.

[3] H. Mizubayashi, Y. Yoshihara, and S. Okuda. *Physica Status Solidi A*, **129**, 1992. p.475.

[4] M. Weller, J. Diehl, and H.-E. Schaefer. *Philosophical Magazine A*, **63** (3), 1991. p.527.

[5] L. B. Freund. *Journal of Applied Mechanics*, **54**, 1987. p. 553.

[6] T. H. Courtney. Mechanical Behavior of Materials. McGraw-Hill: New York, 1990. pp.31, 170, and 224.

[7] W. D. Nix. *Metallurgical Transactions*, **20**A, 1989. p. 2217.

[8] R. Venkatraman and J. C. Brauvman. *Journal of Materials Research*, **7** (8), Aug. 1992. p. 2040.

[9] C. V. Thompson. *Journal of Materials Research*, **8** (2), Feb. 1993. p. 237.

[10] T. Tsakalakos and J. E. Hilliard. *Journal of Applied Physics,* **54** (2), Feb. 1983. p.734.

[11] J. B. Pethica, R. Hutchings and W. C. Oliver. *Philosophical Magazine A*, **48** (4), 1983. p. 593.

[12] L. Maniguet, M. Ignat, M. Dupeux, J. J. Bacmann, and Ph. Normandon. Thin Films: Stresses and Mechanical Properties IV. (Mater. Res. Soc. Symp. **308**). 1993. p. 285.

[13] T. P. Weihs, S. Hong, J. C. Brauvman, and W. D. Nix. *Journal of Materials Research*, **3** (5), Sept./Oct. 1988. p. 931.

[14] K. Najafi and K. Suzuki. *Thin Solid Films*, **181**, 1989. p. 251.

[15] W. H. Chang. *IEEE Transactions on Microwave Theory and Techniques*. Sept. 1976. p.608.

[16] M. E. Thomas, I. A. Saadat, and S. Sekigahama. *IEEE Transactions VMIC Conference*. June 1991. p.116.

[17] D. Halliday and R. Resnick. Physics, Part Two. 3rd ed. John Wiley and Sons: New York. 1978, p. 673.

[18] S. Wang, S. Crary, and K. Najafi. *Materials Research Society Symposium Proceedings*, **276**, 1992. p. 203.

[19] P. Osterberg, H. Yie, X. Cai, J. White, and S. Senturia. MEMS 94, Oiso, Japan.

[20] R. C. Hibbeler. Mechanics of Materials. Macmillan Publishing Company: New York, 19991. p. 609.

[21] P. Osterberg. and S. Senturia. (accepted for publication) 1994 Solid-State Sensor and Actuator Workshop, Hilton Head, South Carolina. June 14-18, 1994.

[22] C. V. Thompson. *Annual Review of Materials Science*, **20**, 1990. p. 245.

[23] M. Ignat, A. Chouaf, and P. Normandon. Thin Films: Stresses and Mechanical Properties II. (Mater. Res. Soc. Symp. **188**). 1990. p. 97.

[24] Metals Handbook 9th Ed., Vol. 3. D. Benjamin and C. W. Kirkpatrick (editors). American Society for Metals: Metals Park, Ohio, 1980. p. 329.

[25] C. E. Morosanu. Thin Films Deposited by Chemical Vapour Deposition. Elsevier: New York, 1990. p. 226.

[26] P. A. Flinn. Thin Films: Stresses and Mechanical Properties I. (Mater. Res. Soc. Symp. **130**). 1989. p. 41.

[27] R. W. Hoffman. Physics of Thin Films, **3**. G. Hass and R. E. Thun (editors), Acedemic Press: New York, 1966. p. 247.

Institute Archives and Special Collections
Room 14N-118
The Libraries
Massachusetts Institute of Technology
Cambridge, Massachusetts 02139-4307

This is the most complete text of the thesis available. The following page(s) were not included in the copy of the thesis deposited in the Institute Archives by the author:

Appendix A : videotape : voltage index

(is included in Archives' copy)

Telephone: (617) 253-5690 • reference (617) 253-5136